Reinterpretation of excited states in ^{212}Po: Shell-model multiplets rather than α-cluster states

A. Fernández,[1] A. Jungclaus,[1,*] P. Golubev,[2] D. Rudolph,[2] L. G. Sarmiento,[2] A. Gargano,[3] H. Naïdja,[4] A. Astier,[5] E. Dupont,[5] A. Gadea,[6] E. Nácher,[1] A. Perea,[1] K. Wimmer,[1] E. Clément,[7] G. Fremont,[7] J. Goupil,[7] C. Houarner,[7] B. Jacquot,[7] A. Korichi,[5] A. Lemasson,[7] H. J. Li,[7] J. Ljungvall,[5] L. Ménager,[7] R. M. Pérez-Vidal,[6] C. M. Petrache,[5] D. Ralet,[7] J. A. Ropert,[7] F. Saillant,[7] A. Såmark-Roth,[2] G. S. Simpson,[8] C. Spitaels,[7] M. Zielinska,[9] S. Ansari,[9] J. Dudouet,[10] A. Illana,[11] M. Jurado,[6] D. Kocheva,[12] N. Lalović,[2] Ch. Lorenz,[2] B. Quintana,[13] G. Rainovski,[12] N. Redon,[10] G. Tocabens,[5] D. Barrientos,[14] G. Benzoni,[15] B. Birkenbach,[16] A. J. Boston,[17] H. C. Boston,[17] A. Bracco,[15,18] M. Ciemala,[19] J. Collado,[20] D. M. Cullen,[21] C. Domingo-Pardo,[6] J. Eberth,[16] V. González,[20] L. J. Harkness-Brennan,[17] H. Hess,[16] D. S. Judson,[17] W. Korten,[9] S. Leoni,[15,18] A. Maj,[19] R. Menegazzo,[22] D. Mengoni,[22,23] C. Michelagnoli,[24] B. Million,[15] D. R. Napoli,[25] J. Nyberg,[26] Zs. Podolyak,[27] A. Pullia,[18,15] P. Reiter,[16] E. Sanchis,[20] O. Stezowski,[10] Ch. Theisen,[9] and J. J. Valiente-Dobón[25]

[1]*Instituto de Estructura de la Materia, CSIC, E-28006 Madrid, Spain*
[2]*Department of Physics, Lund University, SE-22100 Lund, Sweden*
[3]*Istituto Nazionale di Fisica Nucleare, Complesso Universitario di Monte S. Angelo, I-80126 Napoli, Italy*
[4]*Université Constantine 1, Laboratoire de physique mathématique et subatomique (LPMPS), Constantine 25000, Algeria*
[5]*Université Paris-Saclay, CNRS/IN2P3, IJCLab, 91405 Orsay, France*
[6]*Instituto de Física Corpuscular, CSIC-Universitat de Valencia, E-46980 Valencia, Spain*
[7]*GANIL, CEA/DRF-CNRS/IN2P3, Bd Henri Becquerel, BP 55027, F-14076 Caen Cedex 05, France*
[8]*LPSC, Université Joseph Fourier Grenoble 1, CNRS/IN2P3, Institut National Polytechnique de Grenoble, F-38026 Grenoble Cedex, France*
[9]*Irfu, CEA, Université Paris-Saclay, F-91191 Gif-sur-Yvette, France*
[10]*Institut de Physique Nucléaire de Lyon, Université de Lyon, Université Lyon-1, CNRS-IN2P3, F-69622 Villeurbanne, France*
[11]*KU Leuven, Instituut voor Kern- en Stralingsfysica, 3001 Leuven, Belgium*
[12]*Faculty of Physics, St. Kliment Ohridski University of Sofia, 1164 Sofia, Bulgaria*
[13]*Department of Fundamental Physics, University of Salamanca*
[14]*CERN, CH-1211 Geneva 23, Switzerland*
[15]*INFN Sezione di Milano, I-20133 Milano, Italy*
[16]*Institut für Kernphysik, Universität zu Köln, D-50937 Köln, Germany*
[17]*Oliver Lodge Laboratory, The University of Liverpool, Liverpool, L69 7ZE, United Kingdom*
[18]*Dipartimento di Fisica, Università di Milano, I-20133 Milano, Italy*
[19]*The Henryk Niewodniczański Institute of Nuclear Physics, Polish Academy of Sciences, 31-342 Kraków, Poland*
[20]*Departamento de Ingeniería Electrónica, Universitat de Valencia, Burjassot, Valencia, Spain*
[21]*Nuclear Physics Group, Schuster Laboratory, University of Manchester, Manchester, M13 9PL, United Kingdom*
[22]*INFN Sezione di Padova, I-35131 Padova, Italy*
[23]*Dipartimento di Fisica e Astronomia dell'Università di Padova, I-35131 Padova, Italy*
[24]*Institut Laue-Langevin, Grenoble, France*
[25]*Laboratori Nazionali di Legnaro, INFN, I-35020 Legnaro, Italy*
[26]*Department of Physics and Astronomy, Uppsala University, SE-75120 Uppsala, Sweden*
[27]*Department of Physics, University of Surrey, Guildford, GU2 7XH, United Kingdom*

(Received 4 June 2021; revised 1 October 2021; accepted 28 October 2021; published 29 November 2021)

A γ-ray spectroscopic study of ^{212}Po was performed at the Grand Accélérateur National d'Ions Lourds, using the inverse kinematics α-transfer reaction ^{12}C(^{208}Pb, ^{212}Po) ^{8}Be and the AGATA spectrometer. A careful analysis based on $\gamma\gamma$ coincidence relations allowed us to establish 14 new excited states in the energy range between 1.9 and 3.3 MeV. None of these states, however, can be considered as candidates for the levels with spins and parities of 1^- and 2^- and excitation energies below 2.1 MeV, which have been predicted by recent α-cluster model calculations. A systematic comparison of the experimentally established excitation scheme of ^{212}Po with shell-model calculations was performed. This comparison suggests that the six states with excitation energies (spins and parities) of 1744 (4^-), 1751 (8^-), 1787 (6^-), 1946 (4^-), 1986 (8^-), and 2016 (6^-) keV, which previously were interpreted as α-cluster states, may in fact be of positive parity and belong to low-lying

*andrea.jungclaus@csic.es

shell-model multiplets. This reinterpretation of the structure of ^{212}Po is supported by experimental information with respect to the linear polarization of γ rays, which suggests a magnetic character of the 432-keV γ ray decaying from the state at an excitation energy of 1787 keV to the 6_1^+ yrast state, and exclusive reaction cross sections.

DOI: 10.1103/PhysRevC.104.054316

I. INTRODUCTION

It has long been known that the correct description of the properties of the nucleus ^{212}Po requires accounting for effects due to α clustering. Both the α-decay width of the ground state as well as the large experimental $B(E2)$ transition strengths along the ground-state band can only be reproduced when shell-model configurations and α clustering are considered [1–3]. Despite this awareness, it came as a surprise when the existence of "pure" α-cluster states of unnatural parity was proposed in Refs. [4,5]. These are doublets of states with spin and parity assignments of $J^\pi = 4^-$, 6^-, and 8^- (called unnatural-parity doublets, UPDs, throughout this article although arguments for their natural parity will be presented later), decaying via enhanced $\Delta J = 0$, $E1$ transitions to the positive-parity yrast states. These states cannot be described in the standard α-cluster models, which are based on the simple picture of an α cluster moving around the core in its ground state [3]. Soon after the publication of Refs. [4,5], two theoretical studies were presented with the aim to explain the occurrence of unnatural-parity states and their enhanced collectivity [6,7]. In both, couplings between the α cluster and the ^{208}Pb core in its first-excited state, namely the 3^- collective octupole vibration, were considered in order to simultaneously describe natural and unnatural negative-parity states. In Ref. [6], a coupled-channels calculation was performed to obtain excited states of negative parity while in Ref. [7], a particle-vibration coupling scheme was applied to describe the experimentally identified excited states. Both approaches predict the existence of at least one additional, so far unobserved, doublet of states with $J^\pi = 2^-$ (and possibly also additional 1^- states) with excitation energies below 2.1 MeV. These states are expected to decay, in complete analogy to the 4^-, 6^-, and 8^- UPD, via enhanced $E1$ transitions to the first-excited 2^+ state. The experiment described in Refs. [4,5] had no sensitivity to directly fed $2^- \rightarrow 2^+ \rightarrow 0^+$ cascades because a trigger requiring the detection of at least three γ rays in coincidence was employed. It was therefore the main goal of the present experiment to identify these missing α-cluster states. For this purpose, as will be discussed in detail below, reaction-channel selectivity was achieved through charged-particle detection so that data could be recorded using a particle-$\gamma\gamma$ trigger.

The article is structured in the following way: In Section II, the reasoning behind the choice of all experiment parameters is presented and the experimental setup is described. Section III discusses the different steps of the data analysis, including the treatment of the AGATA (Advanced Gamma Tracking Array) data, the experimental determination of the exact geometry of the setup, and the description of the reaction-channel selection. The experimental results regarding the excitation scheme of ^{212}Po and the linear polarization of γ rays are presented in Sec. IV. In Sec. V, the available experimental information is compared with shell-model calculations, the search for candidates for the missing $J^\pi = 2^-$ levels is described, and the negative-parity structure of ^{212}Po is compared with that of ^{148}Gd. The article is closed with conclusions.

II. EXPERIMENT

A. Choice of experiment parameters

The experiment discussed in Refs. [4,5] employed the α-transfer reaction ^{208}Pb(^{18}O, ^{14}C)^{212}Po in normal kinematics and a target thick enough to stop both the target- and projectile-like reaction products. It relied on the high γ-ray efficiency of the EUROBALL IV array which enabled the construction of the excitation schemes of the different reaction products on the basis of triple-γ-ray coincidences. Aiming for the identification of low-spin states decaying via low-multiplicity cascades, for the present experiment an alternative approach has been chosen. The ^{12}C(^{208}Pb, ^{212}Po)^{8}Be reaction in inverse kinematics, in combination with a thin target, provides a high geometrical detection efficiency for the target-like reaction products due to strong kinematical focusing [8,9]. In principle, the identification of the different target-like recoils by appropriate particle detectors provides a high reaction-channel selectivity [8]. However, in a γ-spectroscopic experiment which implies high reaction rates, the correspondingly high rates of elastically scattered target nuclei would lead to a rapid deterioration of the particle detector during the experiment, which can only be avoided by protecting it with an absorber foil. This is the main reason behind the choice of a ^{12}C target for the present experiment. The absorber can be designed such that the two correlated α particles emitted in the almost instantaneous decay of ^{8}Be can pass, to be detected in a particle detector, while heavier target-like recoils are stopped. In addition, the spatial correlation between the two α particles, which are emitted in a cone with a maximum opening angle of

$$\Psi = 2\sin^{-1}\sqrt{\frac{91.8\,\text{keV} + E_x}{K}}, \tag{1}$$

where K is the kinetic energy of the ^{8}Be recoil and E_x its excitation energy, provides a very clean channel selection and thus allows us to relax the condition on the γ-ray multiplicity.

Regarding the choice of the ^{208}Pb beam energy, several aspects have to be considered. The integrated cross section for multinucleon transfer reactions is largest for center-of-mass (CM) energies around the Coulomb barrier, $CB_{\text{CM}} = 58.9$ MeV ($CB_{\text{lab}} = 1079$ MeV) for the system considered

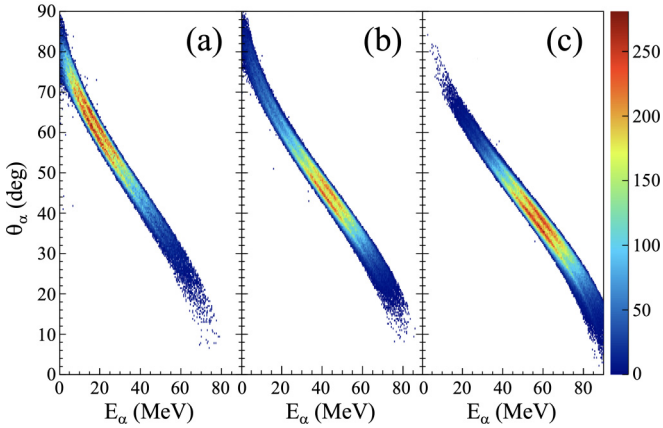

FIG. 1. Monte Carlo simulations of the α-transfer reaction ^{12}C(^{208}Pb, ^{212}Po) ^{8}Be at energies of (a) 3%, (b) 11%, and (c) 20% above the Coulomb barrier. The plots show the polar angle θ_α vs energy E_α matrices for the outgoing α particles. The simulations were performed for a 0.5-mg/cm^2-thick CVD diamond target.

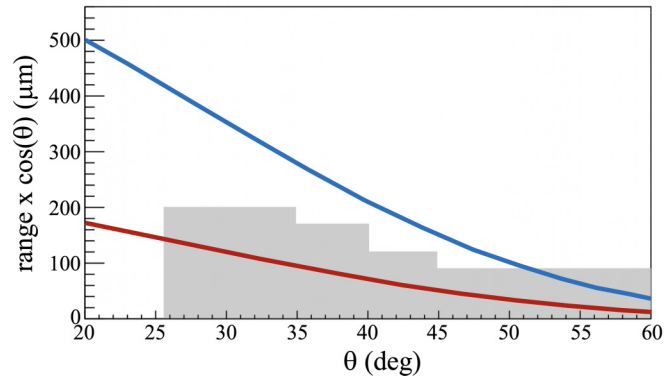

FIG. 2. Ranges in Ta of the elastically scattered carbon ions (red) and the α particles from the ^{8}Be breakup (blue) as a function of the polar angle θ of the carbon and original ^{8}Be nuclei, respectively. The range has been multiplied by cos(θ) in order to account for the angle of incidence. The net Ta thickness of the composite absorber is represented in gray.

here according to the Bass model [10]. However, since the detection of the target-like transfer products is required, the shape of the differential transfer cross section, i.e., the grazing angle of the reaction, has to be taken into account. For the reaction of interest here, ^{12}C + ^{208}Pb, no experimental differential cross-section distributions are available for energies around the Coulomb barrier. However, such distributions have been measured in normal kinematics by Biswas *et al.* for the reaction ^{12}C + ^{232}Th [11] and by Videbaek *et al.* for the system ^{16}O + ^{208}Pb [12]. Assuming that the shape of the cross-section curve and its maximum, at equivalent beam energies with respect to the Coulomb barrier, are similar for all three reactions, Monte Carlo simulations have been performed based on the experimental information from Refs. [11,12], to determine the ranges of polar angles θ_α and kinetic energies E_α of the outgoing α particles. The resulting θ_α-vs-E_α matrices for energies 3%, 11%, and 20% above the Coulomb barrier, respectively, are shown in Fig. 1. In inverse kinematics, the maximum of the cross section is moving towards smaller polar angles with increasing beam energy while the width of the cross-section distribution becomes more narrow. Another important parameter to consider is the excitation energy of the reaction products after the reaction. Under the condition that the classical orbits match before and after the transfer point, a simple formula can be deduced in which the optimum Q value, and thus the excitation energy E_x, only depends on the CM energy and the charge transfer [13]. This simple approach is often used to compare with experimental results [8,14], although these comparisons have shown that its predictive power is limited. For example, for the system ^{12}C + ^{208}Pb at energies 3%–10% below the Coulomb barrier, broad excitation-energy distributions centered around 5.5–8.5 MeV were observed for the CM energies closest to the barrier [14] while nearly zero excitation energy is predicted by the model. Considering that a population at energies above the neutron separation energy, $S_n = 6.008(1)$ MeV [15], will lead mostly to neutron evaporation, the projectile energy should be kept as low as possible in an experiment aiming for γ-ray spectroscopy of ^{212}Po. Based on these two considerations, a ^{208}Pb beam energy of 1187 MeV (5.7 MeV/u), i.e., 10% above the barrier, was chosen for the present experiment.

Another aspect which has to be considered is that a considerable fraction of fusion reactions leading to ^{220}Ra are followed by fission. The fission fragments are confined within a cone whose aperture depends essentially on the available kinetic energy in the CM frame as well as the asymmetry of the fragments and the projectile energy. Since the cross section for fusion-fission reactions is large, it has to be avoided to deposit the fission fragments, and the corresponding radioactivity, in the reaction chamber. Based on the experimental information available for the ^{18}O + ^{208}Pb system [16], a maximum polar angle of 25° was estimated for the fragments of the most asymmetric fission events in inverse kinematics. Hence, particle detection should be limited to polar angles $\theta > 25°$. This is not a limiting factor in view of the simulated θ_α distribution shown in Fig. 1(b).

Finally, as mentioned above, it is necessary to equip the particle detector with an absorber in order to prevent elastically scattered ^{12}C ions from hitting the detector. A simple estimate yields that, assuming a beam intensity of 1 pnA and a carbon target thickness of 0.5 mg/cm^2, ions would be scattered into the relevant angular range $\theta_{\rm lab} = 25°$–$50°$ at a rate of ≈210 kHz. Such a rate would not only damage the detector but also overcharge the data-acquisition system. Figure 2 shows the ranges in Ta (for simplicity ignoring straggling) for the elastically scattered ^{12}C ions and the α particles emitted in the ^{8}Be breakup following the α-transfer reaction as a function of the polar angle. The figure illustrates that by using a single foil of constant thickness it is not possible to stop all carbon ions scattered into the relevant angular range without stopping a considerable fraction of the α particles at the same time. Therefore, the absorber was built by stacking four Ta disks with different radii resulting in a varying thickness as a function of the polar angle. In this way, the net Ta thickness is above the range of the elastically scattered carbon ions and below the range of the α particles. Only for polar angles above

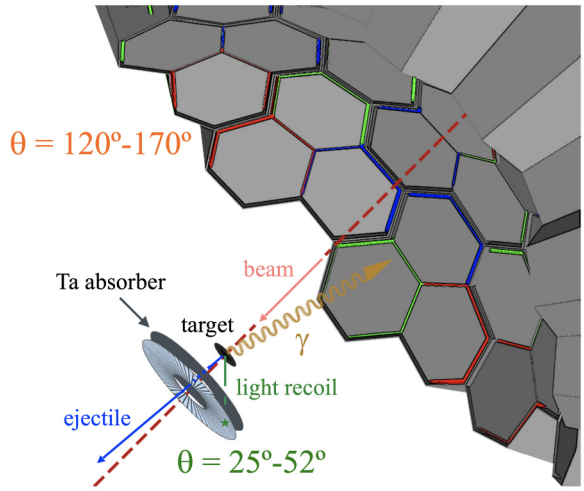

FIG. 3. Sketch of the experimental setup consisting of 12 AGATA triple clusters covering backward angles and the Si DSSSD, protected by a multilayered Ta absorber, placed 34 mm behind the reaction target.

50°–55° does it become increasingly difficult to discriminate between the two species.

B. Experimental setup

The experimental setup consisted of 35 36-fold segmented AGATA crystals [17], arranged in 12 triple clusters (one crystal was missing), placed at a distance of 23.5 cm from the center of the target and covering polar angles in the range $\theta = 120°$–$170°$ [18,19]. For the detection of target-like recoils, a CD-shaped double-sided silicon strip detector (DSSSD) with a segmentation of 32 rings on the n side and 64 sectors on the p side [20] was placed 34 mm behind the target. The DSSSD had a nominal thickness of 310 μm. The inner and outer radii of its active area were 32 and 85 mm, respectively, thus covering the relevant angular range $\theta = 25°$–$52°$. As discussed in the previous section, the DSSSD was covered with a multilayer Ta absorber in order to prevent elastically scattered carbon ions from hitting the Si detector. A sketch of the setup is shown in Fig. 3.

C. Realization of the experiment

The experiment took place at the Grand Accélérateur National d'Ions Lourds (GANIL). The ^{208}Pb beam was accelerated by the cyclotrons of the GANIL accelerator complex and guided to the G1 hall where AGATA was installed. The beam had an average intensity of 2 pnA. The reaction target consisted of a 0.56-mg/cm^2-thin membrane of CVD (chemical vapor deposition) diamond mounted on a Si frame with a free aperture of 6 mm. During most of the 2.5 days of beam time, a particle-$\gamma\gamma$ trigger was used. For 13 hours, however, a particle-γ trigger was employed to allow for the determination of reliable γ-ray intensities despite the presence of isomeric states.

III. DATA ANALYSIS

The analysis of the data taken in this experiment was performed in several steps, as will be discussed in the next sections. First, standard methods were employed to convert the information with respect to the signals detected in the AGATA crystals into the energies and emission angles of the γ rays emitted following the transfer reaction. Then, combining the information from AGATA and the particle detector, the exact geometry of the experimental setup was determined. Finally, the options for a clean selection of the α-transfer channel leading to ^{212}Po were investigated.

A. Processing of the data from AGATA

The processing of the information from the AGATA detectors, from the raw traces to the tracked γ-ray energies and angles of incidence, is carried out in several steps. First, the signal amplitudes of the 36 segments and the central contact (core) of each AGATA crystal are calibrated in energy using the ten most intense γ rays of a ^{152}Eu calibration source. Furthermore, the sampled signals (traces) of the segments are aligned in time with the trace of the core. Cross talk between the segments of a crystal was corrected for using the empirical model described in Ref. [21]. In the next step, the full grid search pulse shape analysis (PSA) algorithm was performed in the offline replay of the data to determine the interaction points of the γ rays in the detector volume. Because most of the AGATA crystals exhibited signs of neutron damage at the time of the experiment, an empirical correction was applied to the core and segment energies to compensate for the loss in charge collection efficiency as function of the interaction position within the crystal [22]. Then, the times of all crystals were aligned. Finally, for each event the energies of the segments within a crystal were renormalized to the respective core energy. Following this preprocessing of the data, the Orsay forward tracking (OFT) γ-ray tracking algorithm [23] was applied to reconstruct the full energy and the interaction points of each γ ray hitting the AGATA array. The relative efficiency of the array was determined by means of a ^{152}Eu calibration source and extrapolated to γ-ray energies up to 2.5 MeV using Monte Carlo simulations. More details about the data processing are provided in Ref. [24].

B. Doppler correction using kinematical reconstruction

To profit from the exceptional position resolution of the AGATA detectors, it is mandatory to determine for each event the velocity β and the scattering angle in the laboratory, θ_L, of the ^{212}Po ion emitting the γ ray to optimize the Doppler correction and thus the energy resolution. The starting point for the calculation of β and θ_L is the reconstruction of the direction of motion of the original ^{8}Be nucleus from the impact positions of the α particles on the DSSSD segments. The energy straggling of the α particles traversing the absorber in front of the DSSSD prevents a reliable determination of the individual momenta of the two α particles after the reaction. Therefore, equality of the absolute values of the momenta is assumed and the azimuthal and polar angles of the ^{8}Be recoil

are determined using the following equations:

$$\sin[\phi(^8\mathrm{Be})] = \frac{\sin(\phi_1)\cos(\theta_1) + \sin(\phi_2)\cos(\theta_2)}{\cos(\theta_1) + \cos(\theta_2)},$$

$$\cos[\theta(^8\mathrm{Be})] = \frac{\cos(\theta_1) + \cos(\theta_2)}{2\cos(\Psi/2)},$$

where ϕ_1, ϕ_2 and θ_1, θ_2 are the azimuthal and polar angles of the two α particles, respectively, and Ψ is the opening angle between them. In the present experiment, opening angles in the range $\Psi < 4^\circ$ are expected (see Sec. III E). Note that the uncertainty in the determination of the ^{8}Be recoil direction is dominated by the limited segmentation of the DSSSD. Even a precise measurement of the α-particle energies would not lead to a significant improvement. The quantities β and θ_L of the ^{212}Po recoil, which are required for the Doppler correction, are then obtained from a Monte Carlo simulation which relates these quantities to $\theta(^8\mathrm{Be})$, taking into account the kinematics of the transfer reaction and the slowing-down of the ions in the target.

C. Determination of the exact geometry

Before proceeding to the analysis of γ-ray spectra, it is crucial to determine the exact geometry of the experimental setup, i.e., to fix the relative positions and orientations of the target, the AGATA array, and the DSSSD. This allows for the best possible Doppler correction and thus an optimum energy resolution. As sketched in Fig. 4(a), the z axis is chosen parallel to the beam direction and the origin of the coordinate system is set at the beam spot on the target. The parameters defining the geometry of the setup are then the position of AGATA, the position of the DSSSD center, and the orientation of one of the DSSSD sectors. First, the orientation of the DSSSD was fixed by inspecting the γ-ray spectra sorted as a function of the rotation parameter ϕ_0 and choosing the value which provides the best energy resolution for γ rays decaying from excited states with negligible lifetimes. This is illustrated in Fig. 4(b). In the next step, the DSSSD position in the xy plane was determined. For this purpose, the energy of the 1680-keV, $2_3^+ \rightarrow 0^+$ transition [25] was determined as a function of the reconstructed azimuthal angle of the ^{8}Be recoil. The best constancy of the transition energy was obtained when the position of the DSSSD was fixed to $x = 1$ mm and $y = 3$ mm, as demonstrated by the χ^2 surface shown in Fig. 4(c). A similar approach was followed to optimize the AGATA position, i.e., the Doppler corrected γ-ray energy was studied as a function of the azimuthal angle of detection. However, in this case the Doppler-corrected energies showed no sensitivity to the position of AGATA in the xy plane so that the latter was set to $x = y = 0$ mm.

The last two parameters to be fixed are the positions of AGATA and the DSSSD in the z direction. Since they are correlated, they have to be determined simultaneously. When the correct positions are used, the Doppler-corrected γ-ray energies (i) do not depend on the polar γ-ray detection angle and (ii) should agree with the literature values. Consequently, the following two parameters were sampled in terms of the z offsets of AGATA and the DSSSD. The first is the squared

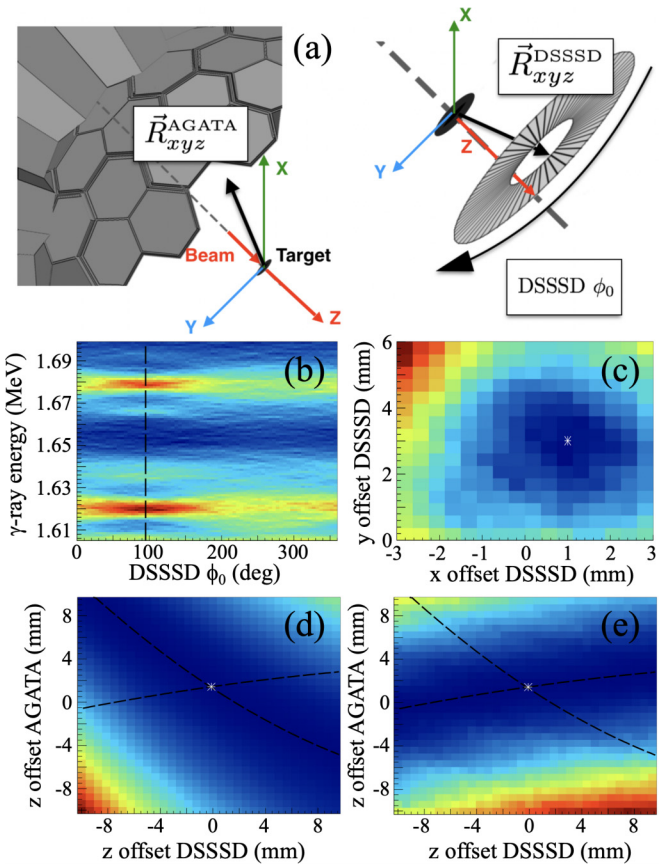

FIG. 4. (a) Sketch of the reference frame for the detector positions. (b) Doppler-corrected γ-ray energy as a function of the DSSSD orientation. (c) χ^2 values measuring the constancy of the Doppler-corrected γ-ray energy as a function of the azimuthal angle of the ^{8}Be recoil. (d), (e) χ^2 matrices for the determination of the z positions of AGATA and the DSSSD, respectively. See text for details.

difference between the γ-ray energies for two groups of detectors, one with $\theta < 135^\circ$ and the other one comprising the most backward crystals with $\theta = 150^\circ$–170°. The other inspected quantity is the squared deviation of the Doppler-corrected γ-ray energy with respect to the literature value. Taking as example again the 1680-keV, $2_3^+ \rightarrow 0_1^+$ transition, pronounced valleys of minimum χ^2 values in terms of the z offsets of AGATA and the DSSSD were found for both parameters. This is illustrated in Figs. 4(d) and 4(e). After a parametrization of these valleys, the optimum values of 1.5 and 0 mm for the z offsets of AGATA and the DSSSD, respectively, were obtained from the intersection. This approach was further validated using the 727-keV, $2_1^+ \rightarrow 0_1^+$ and 432-keV, $6_1^- \rightarrow 6_1^+$ transitions [5] leading to consistent results. Note that the misalignment of the DSSSD evinced in Fig. 4(c) leads to a dependence of the energy of the recoiling ^{8}Be measured in a ring of the Si detector on the azimuthal angle ϕ. This is illustrated in Fig. 5, which shows the energy deposition in ring 15, in coincidence with the most intense γ transitions in ^{212}Po, as a function of $\phi(^8\mathrm{Be})$. This deviation from cylindrical symmetry was accounted for by applying separate cuts on the total energy for different regions of $\phi(^8\mathrm{Be})$, as outlined in the next section.

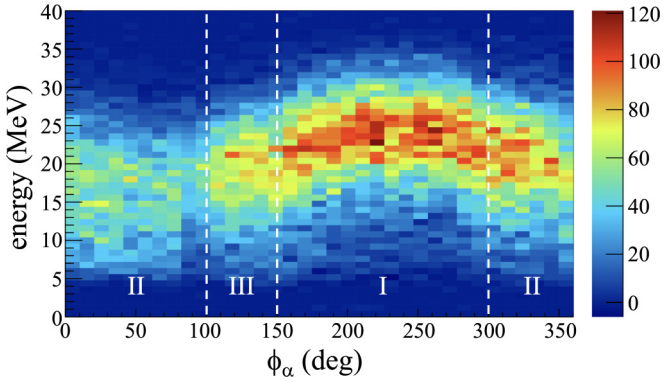

FIG. 5. Total energy measured in ring 15 of the DSSSD in coincidence with the most intense γ transitions in ^{212}Po as function of $\phi(^{8}\mathrm{Be})$. The misalignment of the DSSSD with respect to the actual beam axis breaks the cylindrical symmetry.

D. Selection of the reaction channel

The Ta absorber placed in front of the DSSSD was designed in such a way that no reaction product heavier than ^{4}He could reach the detector. Therefore, only the events corresponding to one of the following four reaction channels were recorded: (i) the $\alpha 2n$ fusion-evaporation channel leading to ^{214}Rn, (ii) the $p2n$ fusion-evaporation channel leading to ^{217}Fr, (iii) the incomplete-fusion reaction $^{12}\mathrm{C}(^{208}\mathrm{Pb}, ^{211}\mathrm{Po})\,^{8}\mathrm{Be}+n$, and finally (iv) the α-transfer reaction populating ^{212}Po, the nucleus of interest. Clean γ-ray energy spectra comprising only those γ rays which belong to one of the two reaction channels with a residual ^{8}Be target recoil are obtained when the detection of particles in two nonadjacent rings of the DSSSD is required. However, this spectrum does not contain the full statistics available for ^{212}Po. Due to the small opening angle between the two α particles the probability for their detection in a single or two neighboring DSSSD rings is rather high. An event-by-event recovery of these events was performed based on the total energy after applying addback on the DSSSD ring energies. The total DSSSD ring energy as a function of the polar angle is shown in Fig. 6 in coincidence with the strongest γ transitions in ^{212}Po, ^{211}Po, and ^{214}Rn, respectively. For ^{212}Po and ^{211}Po, only events with energy depositions in two nonadjacent rings were included. The azimuthal angle ϕ was restricted to the interval 150°–300° (the region labeled I in Fig. 5) to account for the asymmetry of the setup discussed in the last section (corresponding cuts were set for the regions II and III). Applying the energy cut shown as white dashed lines in Fig. 6, about 82% of the ^{212}Po events with both α particles hitting the same or adjacent rings are recovered. At the same time, the ^{214}Rn contamination is kept at a very low level despite its much higher cross section. This procedure allows us to add about 30% statistics to the ^{212}Po spectrum obtained requiring the detection of the two α particles in nonadjacent rings. Note that, although the total-energy distributions for ^{212}Po and ^{211}Po are overlapping as shown in Fig. 6, they are still sufficiently different to allow for an unequivocal assignment of any newly observed γ ray to either of the two reaction channels. The γ-ray spectra obtained considering all events

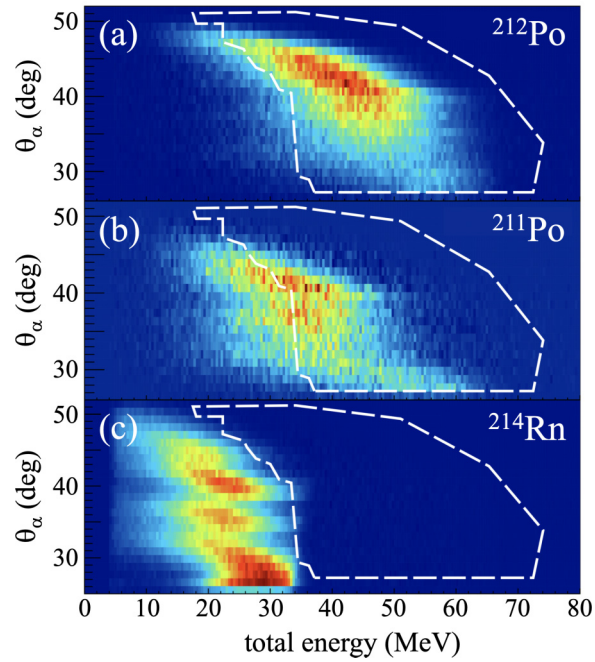

FIG. 6. Total DSSSD ring energy as a function of the polar angle of particle detection in coincidence with known γ transitions in (a) ^{212}Po, (b) ^{211}Po, and (c) ^{214}Rn for $150^\circ < \phi < 300^\circ$, i.e., region I in Fig. 5. In panels (a) and (b), only events with energy depositions in two nonadjacent rings were considered. The region enclosed by the white dashed line was used to recover events belonging to ^{212}Po. See text for details.

with total energies either inside or outside the indicated cut are shown in Fig. 7. This figure shows that a comparison between the two spectra provides a clear discrimination between the γ rays belonging to either ^{212}Po or ^{211}Po.

E. ^{8}Be excitations

In general, the partition of the excitation energy in transfer reactions tends to be governed by the direction of the transferred nucleons. In fact, qualitative agreement with the experimental observables can be achieved within simple semiclassical models of the reaction dynamics [13,26], in which the receptor nucleus is considered to absorb the incoming momentum of the transferred nucleon or cluster. The mass asymmetry between the receptor and the donor also seems to play an important role, in particular at low excitation energy. This was demonstrated, for example, in nucleon-transfer reactions with Li projectiles in normal kinematics [27] and reactions with a ^{238}U beam in inverse kinematics [8], in which little or no excitation of the light reaction product was observed. In the present experiment, due to the use of thick absorbers in front of the DSSSD, the energies of the α particles could not be measured with sufficient precision to allow us to distinguish excitation energy differences of a few MeV. In contrast, owing to the segmentation of the DSSSD, our experimental setup was quite sensitive to the spatial correlation between the two emitted α particles. Using the position information from the rings and sectors of the

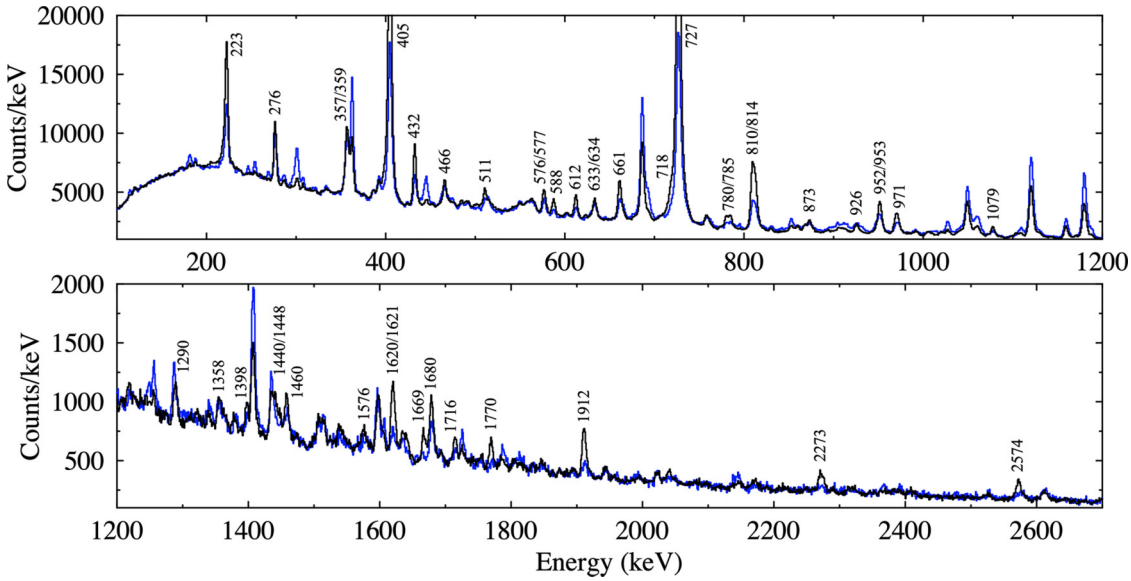

FIG. 7. γ-ray spectra in coincidence with detected particles with total energies inside (black) and outside (blue) the region enclosed by the dashed white line in Fig. 6. The former spectrum has been scaled down to allow for a better comparison. The strongest transitions belonging to ^{212}Po are labeled by their energies in keV. See text for details.

DSSSD, the opening angle between the two α particles, Ψ, was calculated event-by-event. It is shown as a function of the reconstructed polar angle of the recoiling ^{8}Be in Fig. 8. Besides the expected small opening angles, a second band reaching values up to 22° is clearly observed. When the two α particles are emitted from ^{8}Be in an excited state, they are, as compared with emission from the ground state, less focused in forward direction (in the laboratory frame). Also shown in Fig. 8 are the expected maximum opening angles as a function of $\theta(^{8}\text{Be})$ for the decay of the ground and the first two excited states, the 2_1^+ at 3.03 and the 4_1^+ at 11.35 MeV, respectively [28]. We note that the opening angle distributions can reach slightly larger values since both states are resonances with

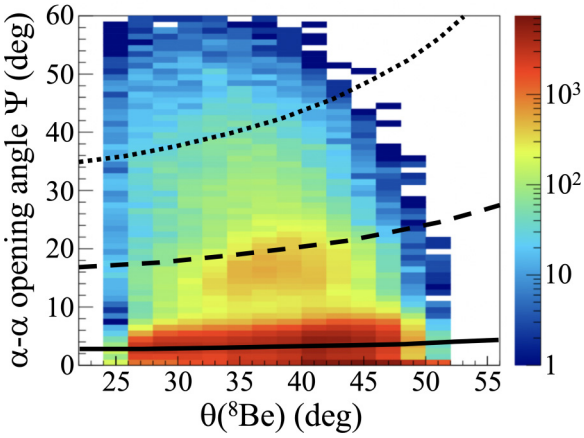

FIG. 8. Opening angle Ψ between the two detected α particles as a function of the reconstructed polar angle θ of the recoiling ^{8}Be. The maximum opening angles Ψ expected for emission from the ground and the 2_1^+ and 4_1^+ states of ^{8}Be, calculated using Eq. (1), are shown as solid, dashed, and dotted lines, respectively.

widths of 1.5 and 3.5 MeV, respectively [28]. Figure 8 suggests that the concentration of events at opening angles around 20° results from ^{8}Be decays from the excited 2_1^+ state at 3.03 MeV. A lower limit for the probability of exciting the ^{8}Be to this state in the transfer reaction was estimated by means of a GEANT4 Monte Carlo simulation of the reaction kinematics and the ^{8}Be decay, considering a detailed description of the geometry including the multilayered Ta stopper. Decays from the 2_1^+ state were simulated by parametrizing the excitation energy using a Breit-Wigner distribution with a width of $\Gamma = 1.5$ MeV. Fitting the experimental opening-angle distributions with simulated ones for several $\theta(^{8}\text{Be})$ slices provided a lower limit of 20% for the excitation probability. However, the real value will probably be much higher considering that the ratio of events with a missing α particle, i.e., an α which escaped through the central hole, reaches 30% in the inner region of the DSSSD.

IV. EXPERIMENTAL RESULTS

A. Extension of the level scheme of ^{212}Po

To study the excitation scheme of ^{212}Po, $\gamma\gamma$-coincidence matrices were generated after selection of the α-transfer channel based on particle energy and multiplicity conditions as described in Sec. III D. Aiming for the identification of new transitions, this approach was found to be the best option, since it significantly reduces the background from fusion-evaporation reactions and, at the same time, eliminates the vast majority of events which would lead to an erroneous kinematical reconstruction. Before inspecting the $\gamma\gamma$-coincidence spectra, the γ-ray singles spectra with inverted cuts on the total particle energies shown in Fig. 7 were compared to check the cleanliness of the gating transitions, taking advantage of the extensive spectroscopic information available for ^{211}Po

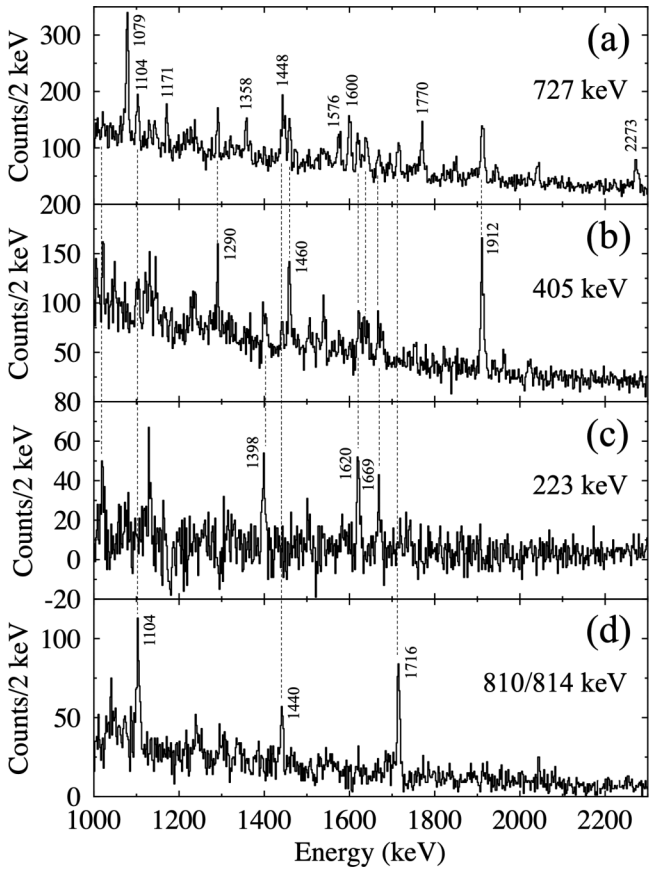

FIG. 9. γ-ray spectra in coincidence with the (a) 727-keV, (b) 405-keV, and (c) 223-keV transitions within the ground-state band. (d) γ-ray spectrum in coincidence with the unresolved doublet consisting of the 810- and 814-keV transitions.

[29]. For the construction of the ^{212}Po level scheme, only γ rays with a statistical significance above 2σ in both coincidence and singles spectra, i.e., those γ rays whose intensity is larger than twice the uncertainty of the latter, were taken into account. Sample spectra in coincidence with the most prominent transitions in ^{212}Po are shown in Fig. 9. The energies and intensities of all γ rays which were observed in the present work and assigned to belong to ^{212}Po are listed in Table I. The excitation scheme constructed on the basis of this information is presented in Fig. 10. In general, good agreement with the excited states previously reported in the literature [1,5,25] is observed. In particular, all low-lying negative-parity states shown in pink and blue in Fig. 6 of Ref. [5] were also observed in the present experiment. They are shown with the same color code in Fig. 10. In the following, we therefore only discuss the γ rays and coincidence relations which led, based on the present data set, to the identification of new excited states. When available, the transition and level energies quoted in Table I and Fig. 10 were adopted from Ref. [5], since that experiment did not suffer from the large Doppler shifts present in the one discussed here. They are thus expected to be more reliable. The energies of other known states were taken from Ref. [25].

Besides the population from the 4^+ member of the ground-state band, the strongest feeder of the 2^+ yrast state is the 810-keV transition decaying from the well-established excited $3^{(-)}$ state at 1537 keV. Three γ rays with energies of 1104, 1440, and 1716 keV are observed in prompt coincidence with this 810-keV, as well as the 727-keV $2^+_1 \rightarrow 0^+$ ground-state transition. Although the spectrum shown in Fig. 9(d) includes all γ rays in coincidence with either component of the 810, 814-keV doublet which is unresolved in the present experiment, see Fig. 7, the energy resolution is sufficient to show that these three transitions are in coincidence with the left part of the doublet, i.e., the 810-keV transition. Since no additional coincidence relations could be established for them, they are assumed to decay from excited states at energies of 2641, 2977, and 3253 keV. We note that the excitation energy of the 2975-keV level proposed by Astier *et al.* [5] differs by only 2 keV from the new 2977-keV state proposed here. Although based on the energy uncertainties and the decay branches it cannot be excluded that the 1620- and 1140-keV γ rays are emitted in the decay of the same level, we assume here that they depopulate two different states. Similarly, since it cannot be proven that the two γ rays with energies of 1290 and 634 keV decay from the same excited state, two levels with an excitation energy of 2421 keV are reported in Fig. 10.

Prominent transitions with energies of 785, 952, and 1079 keV are observed in coincidence with the 727-keV ground-state transition. They correspond to the known decay branches of the $2^+_{2,3,4}$ states to the 2^+_1 level. In the γ-ray singles spectrum shown in Fig. 7, intense lines at energies of 1621 and 1680 keV are present. The former is a doublet, consisting of the known $1^+ \rightarrow 0^+$ transition [28] and the decay of the 2975-keV level to the 6^+ state [5] as evinced by the strong 1620-keV line in the coincidence spectrum of the 223-keV transition shown in Fig. 9(c). The 1680-keV line, on the other hand, corresponds to the known ground-state decay of the 2^+_3 state. We note that the measured branching ratio between the 1680- and 952-keV transitions deexciting the 2^+_3 level is 0.32(6), in agreement with the value of 0.35(10) reported in the literature [28]. Transitions linking the second and fourth 2^+ states with the ground state could not be observed in the present work.

The observation of the decays of the known 1^+ and $2^+_{2,3,4}$ states demonstrates the high sensitivity of the present experiment for decays with low γ-ray multiplicity. As shown in Figs. 9(a)–9(c), several additional lines are visible in the spectra in coincidence with the members of the ground-state band. Based on the observed coincidence relations, various new excited states could be identified. Levels at excitation energies of 1898, 2175, 2303, 2327, 2497, and 3000 keV are proposed based on the observation of γ rays with energies of 1171, 1448, 1576, 1600, 1770, and 2273 keV exclusively in coincidence with the 727-keV ground-state transition. An additional 1358-keV γ ray has been identified as a decay path from the known 2085-keV level to the 2^+_1 state. The observation of γ rays with energies of 1290, 1460, and 1912 keV in coincidence with both the 727- and 405-keV transitions suggests the existence of new excited states at energies of 2421, 2592, and 3044 keV. which are all decaying to the 4^+_1

TABLE I. Energies E_γ and relative intensities I_γ of γ rays observed in the present experiment and assigned to ^{212}Po. The γ-ray energies quoted in Ref. [5] are listed for comparison. Initial- and final-state energies, spins, and parities are adopted from Table 2 of that reference. The members of the supposedly unnatural-parity doublets are printed in bold.

E_γ (keV)	E_γ^{lit}[a] (keV)	I_γ	E_i (keV)	E_f (keV)	J_i^π	J_f^π
222.7(1)	222.6	15.3(7)	1355	1132	6^+	4^+
276.1[b]	276.1*	6(2)	**1751**	1475	**8**	8^+
357.1[b]	357.1	7(3)	1832	1475	10^+	8^+
358.8(5)	358.5	0.4(2)	2103	1744	$5^{(-)}$	4^-
359.2(4)	358.6	0.5(2)	2374	2016	$7^{(-)}$	6^-
371.0(3)	371.0	0.7(3)	2780	2409	10	11^-
405.0(1)	404.9	60(3)	1132	727	4^+	2^+
405.1(2)	405	1.2(4)	1537	1132	$3^{(-)}$	4^+
432.7(1)	432.3*	4.2(4)	**1787**	1355	**6**$^+$	6^+
466.3(1)	465.7	2.7(3)	2003	1537	$4^{(-)}$	$3^{(-)}$
510.9[b]	510.9	1.4(4)	**1986**	1475	**8**	8^+
564.2(5)	563.8*	0.4(2)	2667	2103		$5^{(-)}$
565.7(4)	566.3	0.8(4)	2103	1537	$5^{(-)}$	$3^{(-)}$
575.5(2)	575.6	0.9(2)	2363	1787	6	6^-
577.5(2)	577.1	2.0(2)	2409	1832	11^-	10^+
588.2(2)	587.5	1.8(3)	2374	1787	$7^{(-)}$	6^-
601.6(4)	601.9	0.6(2)	2604	2003	5	$4^{(-)}$
612.7(2)	612.3*	2.3(2)	**1744**	1132	**4**	4^+
632.5(6)	633.2	0.4(2)	2170	1537		$3^{(-)}$
633.4(3)	633.3*	1.2(2)	2465	1832	10^-	10^+
634.4(4)	633.6	0.6(2)	2421	1787		6^-
661.8(2)	661.3*	2.9(2)	**2016**	1355	**6**	6^+
719.2(4)	718.4	1.9(3)	2470	1751	$9^{(-)}$	8^-
727.2(1)	727.1	100(4)	727	0	2^+	0^+
756.9(4)	757.2*	0.5(2)	2860	2103		$5^{(-)}$
758.4(4)	758.4	0.5(3)	2295	1537		$3^{(-)}$
780.9(2)	780.4*	1.0(1)	3155	2374	$7^{(+)}$	$7^{(-)}$
785.7(3)	785.4(1)[c]	2.2(3)	1513	727	2^+	2^+
809.6(1)	809.7	10.5(7)	1537	727	$3^{(-)}$	2^+
813.7(1)	813.6*	4.5(2)	**1946**	1132	**4**	4^+
853.2(2)	853.4	0.4(1)	2604	1751		8^-
868.4(4)	868.4	0.7(2)	2700	1832	12^+	10^+
873.5(3)	873.1	1.1(2)	2228	1355	7	6^+
926.0(2)	926.2	0.6(3)	2281	1355		6^+
952.3(3)	952.12(1)[c]	3.8(3)	1679[c]	727	2^+	2^+
952.7(2)	953.1	1.8(2)	2085	1132	(4^+)[c]	4^+
971.4(3)	971.1[e]	<4.5	2103	1132	$5^{(-)}$	4^+
1005.8(4)	1005*	0.4(2)	2837	1832		10^+
1021.2(4)	1020	0.3(1)	2374	1355	$7^{(-)}$	6^+
1049.4(4)	1049*	0.3(1)	2881	1832		10^+
1078.4(2)	1078.6(1)[c]	1.6(2)	1806[c]	727	2^+	2^+
1104.1(4)		0.4(2)	2641	1537		$3^{(-)}$
1171.2(6)		0.6(3)	1898	727	(3^+)[d]	2^+
1290.1(4)		0.7(2)	2421	1132		4^+
1357.6(5)		0.4(2)	2085	727	(4^+)[d]	2^+
1398.1(6)		0.9(4)	2753	1355		6^+
1440.3(5)		0.3(1)	2977	1537		$3^{(-)}$

TABLE I. (*Continued.*)

E_γ (keV)	$E_\gamma^{\text{lit}a}$ (keV)	I_γ	E_i (keV)	E_f (keV)	J_i^π	J_f^π
1448.2(7)		1.1(4)	2175	727		2^+
1459.5(5)		0.6(2)	2592	1132		4^+
1575.7(7)		0.7(3)	2303	727		2^+
1600.3(4)		1.2(3)	2327	727		2^+
1620.6(2)	1620.5(1)[c]	1.6(3)	1621[c]	0	1^+	0^+
1621.0(7)	1620*	0.6(3)	2975	1355		6^+
1669.2(8)	1669*	0.4(2)	3024	1355		6^+
1679.7(1)	1679.7(5)[c]	1.2(2)	1679[c]	0	2^+	0^+
1715.8(5)		0.5(1)	3253	1537		$3^{(-)}$
1770.3(4)		1.0(2)	2497	727		2^+
1912.3(4)		1.6(2)	3044	1132		4^+
2272.6(7)		0.9(2)	3000	727		2^+
2574.0(2)		1.0(2)	2574	0		0^+

[a]Uncertainties typically between 0.1 and 0.5 keV and for transitions marked by an asterisk up to 2 keV [5].
[b]Adopted from Ref. [5].
[c]Adopted from Ref. [25].
[d]J^π proposed in the present work.
[e]Part of a doublet [5] which is unresolved in the present work.

level. The intense 1398-keV line visible in Fig. 9(c) gives rise to the existence of a new excited state at an energy of 2753 keV. Finally, a strong 2574-keV line is observed in the γ-ray singles spectrum. Based on the method discussed in Sec. III D, it is unequivocally assigned to ^{212}Po. Since no coincidences with this line could be established, it is assumed to decay from an excited state with the same energy. This conclusion is supported by the fact that the 2273-keV transition, which in the singles spectrum has about the same intensity as the 2574-keV line, is clearly observed in coincidence with the 727-keV ground-state transition.

All remaining transitions placed in the level scheme shown in Fig. 10 agree with the previously published data. Due to the use of a thin target, in the present experiment the γ-ray transitions directly feeding the 8^+ isomer ($T_{1/2} = 14.6(3)$ ns [25]) could not be observed in coincidence with the members of the ground-state band. Their intensities were therefore determined from the γ-ray singles spectrum and, if necessary, corrected for contaminant lines belonging to ^{211}Po. This applies to the 276, 511, and 357-keV transitions which depopulate the 8^- doublet levels and the 10^+ yrast state. No additional transitions possibly feeding the isomeric state and

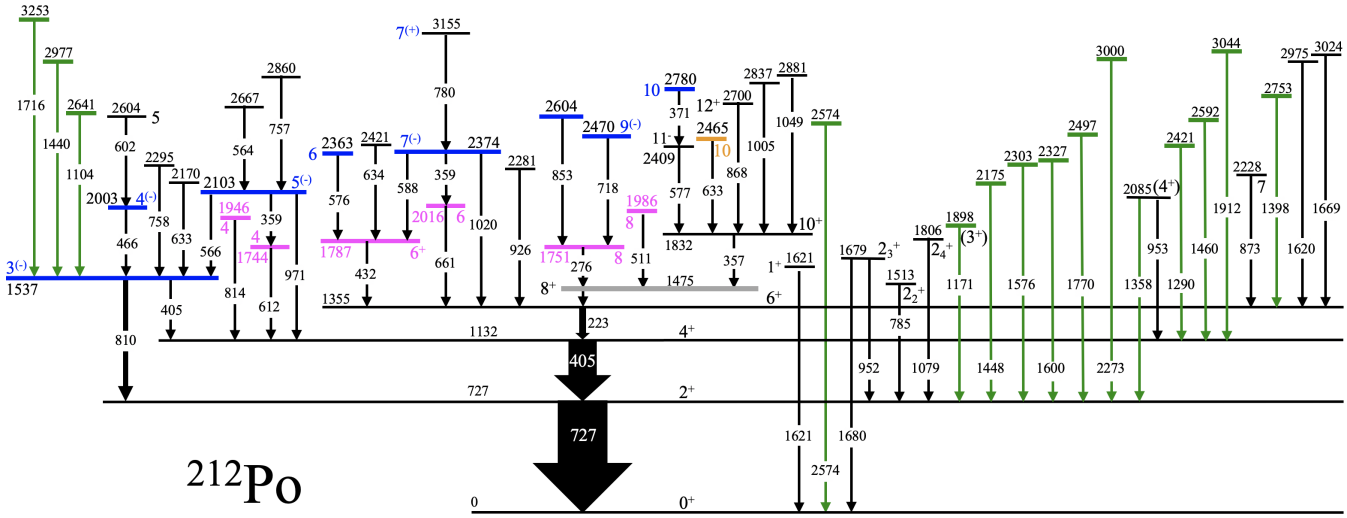

FIG. 10. Partial excitation scheme of ^{212}Po. Newly identified γ rays and excited states are shown in green. Following the color code introduced in Ref. [5], the negative-parity states discussed in the text are highlighted in pink, blue, and orange. Note that in the present work, the negative parity of the UPD shown in pink is questioned. The isomeric 8^+ state at 1476 keV ($T_{1/2} = 14.6(3)$ ns [25]) is shown as thick gray line. When available, the transition and level energies as well as spin assignments were adopted from Ref. [5].

consistent with the adopted significance criterion have been observed.

B. Linear polarization

In Ref. [5], based on the experimental information with respect to angular distributions, angular correlations, and anisotropy ratios R_{ADO}, the γ-ray transitions linking the doublet states with spins of 4 (1744 and 1946 keV), 6 (1787 and 2016 keV), and 8 (1751 and 1986 keV), respectively, as well as the 2465-keV level with spin $J = 10$, to the yrast band were considered to be either stretched $\Delta J = 2$ quadrupole or pure nonstretched $\Delta J = 0$ dipole transitions. Note that these two options cannot be distinguished on the basis of angular distributions. In the case of the 1787-keV state, a spin of 8^+ was excluded since feeding from the 2103-keV, $J = 5^{(-)}$ level was observed leaving a spin of 6 as only possible choice. Then, $\Delta J = 0$ was assumed also for the transitions linking the remaining doublet states to the ground-state band. The assignment of negative parity, however, is not supported by any experimental information. The measured conversion coefficients of 0.37(7) and 0.13(3) for the 276- and 432-keV transitions, respectively, are actually closer to the theoretical values for $M1$ (0.635 and 0.188) rather than $M1$ (0.038 and 0.014) multipolarity [5]. A measurement of the linear polarization of the γ rays linking the UPD to the yrast states would allow us to fix their electric or magnetic character and thus the parity of the UPD. In Ref. [5], such an analysis was performed but the linear polarization could only be measured for the three most intense γ rays confirming $E2$ character of the transitions within the $6^+ \rightarrow 4^+ \rightarrow 2^+ \rightarrow 0^+$ yrast sequence. The position sensitivity of the highly segmented AGATA detectors used in the present experiment in principle allows us to perform continuous-angle Compton polarimetry [30]. However, the maximum degree of polarization is observed at an angle of $\theta = 90^\circ$ with respect to the quantization axis, i.e., the beam axis in the present case. Therefore, in the present experiment the sensitivity to polarization effects is rather limited because the AGATA detectors only covered the angular range $\theta = 120^\circ$–170° (see Sec. II B). Nevertheless, given the importance of this question for the interpretation of the structure of ^{212}Po, an attempt was made to evaluate possible polarization effects in the present data set. The experimental linear polarization is defined as

$$P(\theta) = \frac{1}{Q}\frac{N(\theta, \phi_C = 90^\circ) - N(\theta, \phi_C = 0^\circ)}{N(\theta, \phi_C = 90^\circ) + N(\theta, \phi_C = 0^\circ)}, \qquad (2)$$

where Q is the polarization sensitivity, which is a function of the γ-ray energy, and $N(\theta, \phi_C = 0^\circ)$ and $N(\theta, \phi_C = 90^\circ)$ are the number of events in which the γ ray is scattered parallel and perpendicular to the reaction plane, respectively. The sensitivity of the Compton effect to the linear polarization decreases with the γ-ray energy and is largest for polar Compton-scattering angles θ_C around 90°. Since the positions of the first and second interactions of a γ ray hitting the AGATA array are reconstructed by the tracking algorithm, the polar and azimuthal Compton-scattering angles can be calculated event by event with a precision which is determined by the position resolution and the quality of the tracking. Although integrating the data over appropriately chosen angular ranges provides γ-ray spectra with sufficient statistics, a good compromise has to be found between polarization sensitivity and counting rate. Here, spectra obtained with two different conditions on the polar angle are compared. In the first case, only γ rays emitted at $\theta = 120^\circ$–140° with respect to the beam axis are considered while in the second the full range covered by AGATA in the present experiment is employed. The polar Compton-scattering angle was chosen in the interval $\theta_C = 90 \pm 40^\circ$ to cover the range of highest sensitivity [24,30] while for the azimuthal Compton-scattering angle intervals of $\pm 20^\circ$ around $\phi_C = 0^\circ$, 180° and $\phi_C = 90^\circ$, 270° are considered. The resulting γ-ray spectra, corrected for the instrumental asymmetry determined with a ^{152}Eu calibration source, are shown in Figs. 11(a) and 11(b). A quantitative determination of the experimental linear polarization, which would require a precise characterization of the energy-dependent instrumental polarization sensitivity Q is precluded by the rather limited counting statistics accumulated in the present experiment. Nevertheless, counting-rate differences are clearly discernible for both the 405-keV, $4_1^+ \rightarrow 2_1^+$ and 432-keV γ rays. The latter corresponds to the nonstretched dipole transition depopulating the 1787-keV state with a spin of 6 to the 6_1^+ level. For both lines, the spectra shown in Figs. 11(a) and 11(b) consistently suggest $P(\theta) > 0$. Theoret-

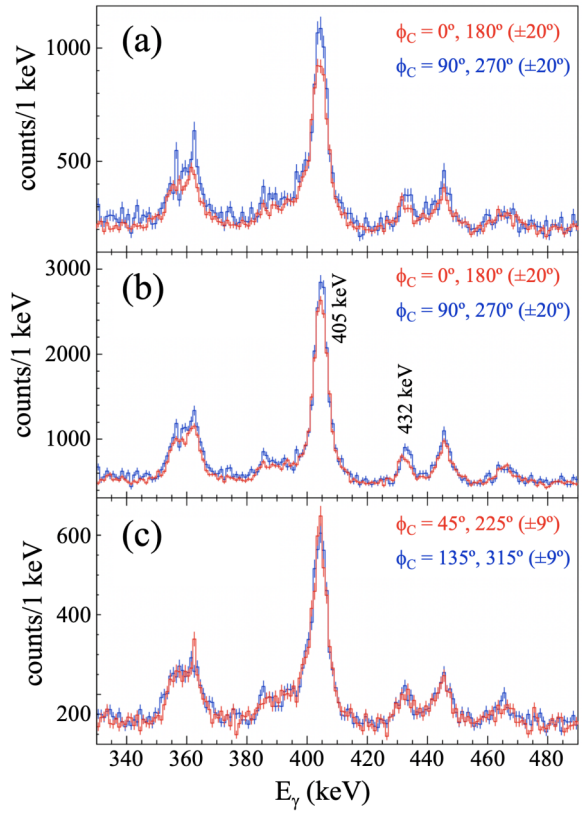

FIG. 11. γ-ray energy spectra for ^{212}Po. The polar Compton-scattering angle was limited to the interval $\theta_C = 90 \pm 40^\circ$. The ranges of the azimuthal Compton-scattering angle ϕ_C are quoted in each panel of the figure. The polar angle θ was limited to $120^\circ < \theta < 140^\circ$ in panels (a) and (c) and unrestricted in panel (b).

ically, positive values of the linear polarization are expected for stretched $E2$ and nonstretched $M1$ transitions, while nonstretched $E1$ are characterized by negative values of $P(\theta)$ [31]. Although the counting statistics is rather limited, the differences between the yields for Compton scattering parallel or perpendicular to the reaction plane evinced in Figs. 11(a) and 11(b) clearly suggest the 432-keV γ ray to be a nonstretched magnetic dipole transition rather than a nonstretched $E1$ as proposed in Ref. [5]. Consequently, a spin-parity assignment of 6^+ is proposed for the 1787-keV level.

To check the soundness of the approach, additional spectra were produced considering intervals of $\pm 20^\circ$ around $\phi_C = 45^\circ, 225^\circ$ and $\phi_C = 135^\circ, 315^\circ$, respectively. They are shown in Fig. 11(c). For these ranges of the azimuthal Compton-scattering angle, no sensitivity with respect to the linear polarization is expected. Indeed, no significant counting-rate differences are observed. The reliability of the present analysis was further investigated on the basis of the 1621-keV, $1^+_1 \rightarrow 0^+_1$ stretched $M1$ transition in ^{212}Po and several well-established γ rays belonging to ^{211}Po (see Ref. [24] for further details). Unfortunately, due to the limited counting statistics and, in some cases, contaminations, it was not possible to determine the sign of the linear polarization also for the other γ rays emitted in the decay of the doublet states. It seems highly desirable to unequivocally determine the character of all nonstretched dipole transitions, and thus the parity of the pretended α-cluster states under discussion, in a dedicated experiment.

V. DISCUSSION

A. Search for theoretically predicted 2^- states

In Refs. [4,5], the supposed unnatural-parity doublets with spins of 4^-, 6^-, and 8^- (shown in pink in Fig. 10) were interpreted as a unique manifestation of α-cluster correlations in ^{212}Po on the basis of the measured lifetimes. Soon after the stunning experimental results were published, two theoretical works were presented aiming for a simultaneous description of both natural and unnatural negative-parity states and trying to provide an explanation for the enhanced collectivity of these states [6,7]. The models presented in these articles describe reasonably well the almost degenerate excitation energies of the experimentally observed UPD and thus seem to corroborate their interpretation. However, the experimental information regarding the linear polarization of the 432-keV γ ray presented in the last section contradicts the assignment of negative for one state and seriously questions this assignment for the other members of the three UPD. It would therefore be very important to verify other predictions made by these models.

Both calculations predict the existence of additional 1^- and 2^- states with a structure similar to that of the UPD. The 2^- states are expected to decay via enhanced $E1$ transitions to the 2^+_1 state, in complete analogy to the decay of the other UPD. As mentioned in the introduction, in the experiment discussed in Refs. [4,5] the observation of directly populated $2^- \rightarrow 2^+ \rightarrow 0^+$ $\gamma\gamma$ cascades was impeded by the use of a triple-γ trigger. In the present experiment, however, there is no technical argument which could explain the nonobservation of the decays of these predicted 2^- states. Therefore, we will discuss in the following whether some of the newly identified excited states (shown in green in Fig. 10) could be valid candidates for the missing UPD with $J^\pi = 2^-$.

Six of the new states, namely those at 1898, 2175, 2303, 2327, 2497, and 3000 keV, decay exclusively to the 2^+_1 state. Considering this decay pattern they, in particular the first ones in the list, could be candidates for the theoretically predicted 2^- states. However, the direct population of these states, ranging from 0.6(3) in relative units for the 1898-keV level to 1.1(4) for the state at 2175 keV (see Table I), is much smaller than expected. The α-transfer reaction used in the present experiment in general favors the population of low-spin states. This is indeed reflected in the observed excitation pattern and the preference for low-multiplicity cascades. These features are understood in a semiclassical approach as a dwindling of the angular-momentum mismatch between the entrance and exit channels resulting from the transfer of charge [32–34]. For the present case, an optimum angular-momentum transfer around $2\hbar$ is estimated. Considering the cross sections measured for the UPD with spin 4, 4.5(2), and 1.9(3), the weak direct population of the newly identified states does not support their assignment as 1^- or 2^- states with similar structure as the UPD. To summarize, the analysis of the data taken in the present experiment does not provide any evidence for the existence of 2^- states in ^{212}Po, at least in the excitation-energy range $E_x \leqslant 3$ MeV, which are similar in structure to the UPD identified in Refs. [4,5] and decay via $E1$ transitions to the 2^+_1 yrast state.

B. Negative-parity states in ^{212}Po and ^{148}Gd

The work of Delion *et al.* [7] was stimulated by the apparent similarity stressed in Ref. [5] between the negative-parity sequences in ^{212}Po and ^{148}Gd. Negative-parity states in ^{212}Po are described as two-neutron excitations of positive parity coupled to the collective octupole phonon state [7]. To reproduce the measured large $E1$ transition probabilities, a cluster component was added to the shell-model wave functions, as had been done in the past in the calculation of the α-decay width from the ^{212}Po ground state [2]. All relevant parameters were adjusted to known excited-state energies. In view of the absence of experimental evidence for the existence of the missing states predicted by theory, we will in the following reconsider the comparison between these two nuclei.

As discussed in detail by Piiparinen *et al.* [35] (see in particular Fig. 10 of that article), in the $N = 84$ nucleus ^{148}Gd the coupling of the two valence neutrons in the $1f_{7/2}$ shell to the collective 3^- state of the ^{146}Gd core gives rise to a complex family of altogether twenty negative-parity levels. In the case of harmonic vibrations, these states would be grouped into multiplets at excitation energies given by the 3^- phonon energy of the core and the $1f^2_{7/2}$ spectrum. This is sketched in Fig. 12(a). Of course, particle-phonon coupling will lead to deviations from this simple picture. The lowest single-particle configuration of negative parity, namely, the $1f_{7/2} \times 0i_{13/2}$ configuration, has an unperturbed energy of 3.74 MeV, i.e., 1.38 MeV above the unperturbed $3^- \times 2^+$

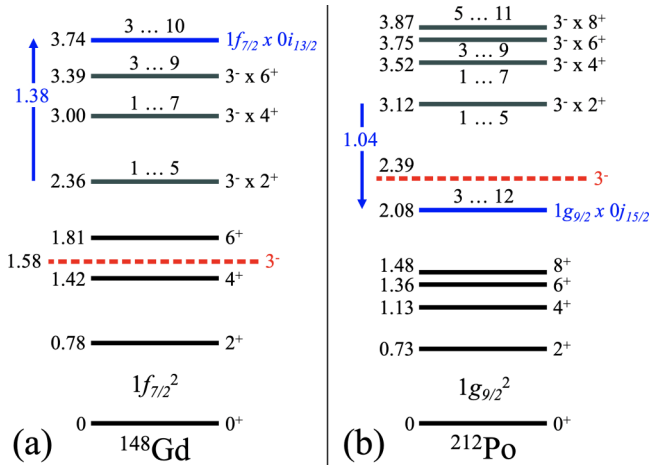

FIG. 12. (a) Members of the $1f_{7/2}^2$ multiplet (black) and unperturbed energies of the $1f_{7/2}^2 \times 3^-$ states (gray) in ^{148}Gd. The position of the 3^- phonon state in the ^{146}Gd core is indicated by a red dashed line while the unperturbed position of the $1f_{7/2} \times 0i_{13/2}$ multiplet is shown in blue. (b) Members of the $1g_{9/2}^2$ multiplet (black) and unperturbed energies of the $1g_{9/2}^2 \times 3^-$ states (gray) in ^{212}Po. The position of the 3^- phonon state in the ^{210}Po core is indicated by a red dashed line while the unperturbed position of the $1g_{9/2} \times 0j_{15/2}$ multiplet is shown in blue. The numbers above the gray and blue lines indicate the spin range of the multiplets.

multiplet, see Ref. [35]. There, it was shown that, even taking into account the anharmonicities of the phonon-coupled states, as well as the residual interaction between the two neutrons of the $1f_{7/2} \times 0i_{13/2}$ configuration, the octupole-coupled states still dominate the negative-parity spectrum at low excitation energy.

In ^{212}Po, one major neutron shell above, the relevant neutron orbitals are those with one unit larger quantum numbers ℓ and j. The ground-state sequence is formed by the $1g_{9/2}^2$ configuration. At negative parity the multiplet which is expected to be lowest in energy is $1g_{9/2} \times 0j_{15/2}$. Based on the apparent similarity between the excited-state energies of the lowest negative-parity states in ^{148}Gd and ^{212}Po as a function of spin (see Fig. 16 of Ref. [5]), it was concluded that, also in ^{212}Po, these states are based on the coupling between the two valence neutrons and the octupole phonon. However, as illustrated in Fig. 12, the situation is actually very different in the two nuclei. First, the excitation energy of the collective 3^- state in ^{210}Po is roughly 0.8 MeV higher as compared with that of the 3^- state in ^{146}Gd. Second, the energy of the lowest two-neutron configuration, $1g_{9/2} \times 0j_{15/2}$, which was estimated following the approach proposed by Piiparinen *et al.* [35] and using the experimental energy of the $\nu 0i_{11/2} \times \nu 0j_{15/2}$, 13^- state, is 1.7 MeV lower than that of the $1f_{7/2} \times 0i_{13/2}$ multiplet in ^{148}Gd. As a consequence, in the case of ^{212}Po, the unperturbed energy of the two-neutron configuration is more than 1 MeV lower than that of the unperturbed $3^- \times 2^+$ multiplet. As shown in Fig. 12, the situation is thus opposite to that encountered in ^{148}Gd.

Although the different configurations are expected to interact and mix, it is natural to assume that in ^{212}Po, in contrast to the situation in ^{148}Gd, the low-lying states of negative parity are strongly influenced by the shell-model configurations. We therefore considered it appropriate to perform a complete set of shell-model (SM) calculations and to compare the results to the available experimental information.

C. Shell-model calculations

Shell-model calculations were carried out using the code ANTOINE [36,37]. The valence space comprised the $0h_{9/2}$, $1f_{7/2}$, $0i_{13/2}$, $1f_{5/2}$, $2p_{3/2}$, $2p_{1/2}$ proton and the $1g_{9/2}$, $0i_{11/2}$, $0j_{15/2}$, $2d_{5/2}$, $3s_{1/2}$, $1g_{7/2}$, $2d_{3/2}$ neutron orbitals. Two different effective interactions were employed, namely, the Kuo-Herling interaction [38] modified by Warburton and Brown [39], commonly named KHPE, and the recently introduced H208 interaction [40,41]. For the calculation of transition probabilities and γ-ray branching ratios, effective charges of $e_\pi = 1.5e$, $e_\nu = 0.8e$ ($e_\pi = 1.5e$, $e_\nu = 0.5e$) were used in the calculations with the KHPE (H208) interaction. With respect to the effective g factors, the values proposed by Arima *et al.* [42], i.e., $g_l^\pi = 1.13$, $g_s^\pi = 3.536$, $g_l^\nu = -0.08$, $g_s^\nu = -2.026$, were used in the KHPE calculations while in those performed with the H208 interaction values of $g_l^\pi = 0.851$, $g_s^\pi = 5.426$, $g_l^\nu = 0.004$, $g_s^\nu = -1.024$ were employed. In the following, we compare the predicted excitation energies, separately for negative and positive parity, to the available experimental information. Thereafter, the discussion will be extended to the electromagnetic decay properties.

1. Negative-parity excitation spectrum

The excitation spectrum of ^{212}Po calculated using the KHPE interaction is shown in Fig. 13. States sharing a >50% main component of the wave function are connected by dashed lines in order to clarify the structure. At negative parity, as expected based on the single-particle energies of protons and neutrons in the valence space, the calculation predicts the neutron $1g_{9/2} \times 0j_{15/2}$ multiplet to form the yrast sequence up to spin 10^-. The next two calculated multiplets, based on the proton $0h_{9/2} \times 0i_{13/2}$ and the neutron $0i_{11/2} \times 0j_{15/2}$ configurations, show the typical parabolic shape with strongly lowered energies for the maximal aligned spin couplings leading to states with spins of $J = j_1 + j_2$ and $J = |j_1 - j_2|$.

In Fig. 13(b), the calculated spectrum is compared with the experimentally observed negative-parity states shown in blue in Fig. 6 of Ref. [5] and in Fig. 10, and the 11^- and 13^- yrast states at energies of 2409 and 2769 keV [5], respectively, which are shown as red lines. The latter two states are observed roughly 100 keV above the predicted maximum-spin levels of the $\pi h_{9/2} \times 0i_{13/2}$ and $\nu 0i_{11/2} \times 0j_{15/2}$ multiplets. With respect to the states in the spin range 3^- to 9^-, a significant difference between the calculated and experimental excitation energies is observed which decreases with increasing spin. On the other hand, we note that the odd-even spin staggering is very similar for the two sets of states. As discussed in Sec. V B, at negative parity mixing between the shell-model multiplets and the octupole-coupled states, $1g_{9/2}^2 \times 3^-$, is expected to occur. This mixing will push the first-excited state of each spin to lower energies. The 3^- state

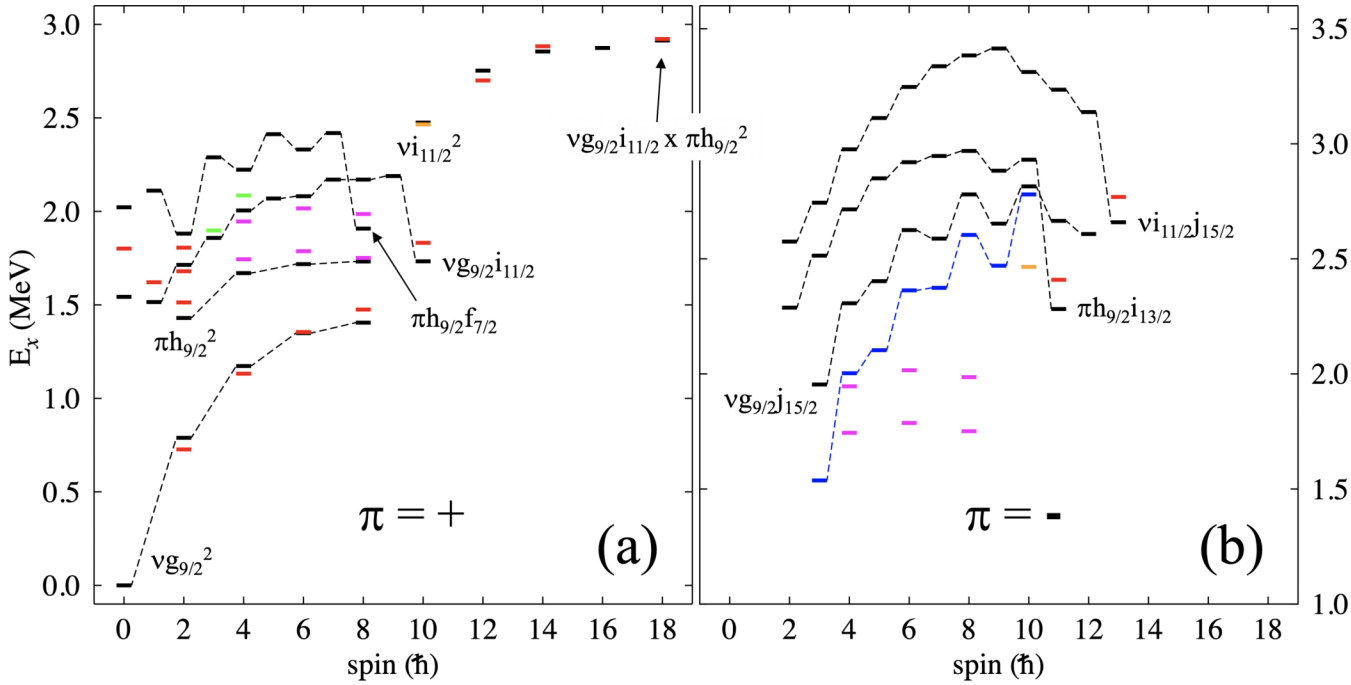

FIG. 13. Comparison between calculated (black) and experimental (colored) excited states of (a) positive and (b) negative parity in ^{212}Po. The results of the calculations performed with the KHPE interaction are presented. Calculated states sharing a >50% main component of the wave function, as well as the experimentally established levels shown in blue in Fig. 10, are connected by dashed lines.

is calculated 420 keV higher in excitation energy than experimentally observed. Roughly the same difference, namely, 380 keV, is observed between the calculated and measured 3^- energies in ^{210}Pb [43], which has the same two-neutron spectrum as ^{212}Po. The shift towards lower energies will be larger for low-spin states since the $3^- \times 2^+$ (1^-,..., 5^-) and $3^- \times 4^+$ (1^-, ..., 7^-) multiplets are lowest in energy and therefore will mix in more strongly than the $3^- \times 6^+$ (3^-, ..., 9^-) and $3^- \times 8^+$ (5^-,..., 11^-) couplings (compare Fig. 12). Figure 13(b) shows that this qualitative theoretical expectation is in good agreement with the experimental findings. In contrast, the theoretical spectrum does not offer any natural explanation for the occurrence of the UPD with spins of 4^-, 6^-, and 8^- and energies in the range 1.7–2.0 MeV (shown in pink). Actually, within the framework of the shell model, no additional negative-parity states in this spin range are expected below 2.7 MeV.

2. *Positive-parity excitation spectrum*

Turning to the positive-parity states, Fig. 13(a) shows the excitation spectrum calculated with the KHPE interaction. Experimental states with firm spin and parity assignment [25] are included for comparison as red lines. A very good agreement between calculation and experiment is observed for the yrast sequence up to the highest spins. Note that, for example, the energy of the α-decaying 18^+ isomer is reproduced within 16 keV. For the known 1_1^+ and $2_{2,3,4}^+$ states, the difference between the calculated and observed energies is slightly larger but with at most 100 keV still acceptable. Only the energy of the 0_2^+ state, with the neutron pair excited from the $1g_{9/2}$ to the $0i_{11/2}$ orbital as a leading configuration, is clearly underestimated by the calculations.

Given the overall good agreement between calculation and experiment for the positive-parity yrast and the excited 2^+ states, the question emerges why none of the 4_2^+, 6_2^+, and 8_2^+ states, which are predicted at energies below 1.8 MeV, were observed, either in the experiment reported in Refs. [4,5] or in the one described here. Recalling that the supposed 4^-, 6^-, and 8^- UPDs with energies in the range 1.7–2.0 MeV cannot be accommodated by the shell model assuming negative parity, we compare them in Fig. 13(a) to the calculated levels of positive parity. Interestingly, the energies of the 4_1^-, 6_1^-, and 8_1^- states, namely 1744, 1787, and 1751 keV [4,5], respectively, are only slightly higher as those of the calculated 4_2^+, 6_2^+, and 8_2^+ levels, which are predicted at energies of 1670, 1718, and 1732 keV. Similarly, the energies of the 4_2^-, 6_2^-, and 8_2^- states proposed in Refs. [4,5] differ by less then 80 keV from those of the calculated 4_3^+, 6_3^+, and 8_3^+ levels, as can be seen in Fig. 13(a). As was shown in the past, the KHPE interaction used here nicely describes the positive-parity spectrum of ^{210}Pb [43] and the experimentally observed 2^+ states in ^{210}Po [44]. The comparison between the shell-model predictions and the excitation energies of the experimentally identified states, see Fig. 13, clearly shows that a very consistent picture is obtained when positive parity is assumed for all six members of the supposed UPD.

To end this section, it is worth mentioning that the energy of the state at 2465 keV, which was assigned $J^\pi = 10^-$ in Refs. [4,5] (shown in orange in Fig. 13 and in Fig. 5 of Ref. [5]), coincides with the calculated energy of the 10_2^+ state, which is based on the fully aligned neutron $0i_{11/2}^2$ configuration, while it is 350 keV lower than the energy of the calculated 10_1^- state. Finally, we note that, based on the calculated excitation energies shown in Fig. 13, $J^\pi = 3^+$ and

4^+ may tentatively be proposed for the newly identified state at 1898 keV and the 2085-keV level, respectively (shown in green in Fig. 10).

3. Comparison between calculated and measured transition probabilities and γ-ray branching ratios

Besides plain excitation energies, another quantity which can be used to associate experimental with calculated states is the γ-ray branching ratio in the decay of an excited state. The first step in the calculation of electromagnetic decay properties within the shell-model approach is the choice of the effective operators. As discussed in the literature, this is for several reasons not a simple task. With respect to the $E2$ transitions, it was shown that it is not possible to reproduce the measured $B(E2)$ values for the $2_1^+ \rightarrow 0_1^+$ and $8_1^+ \rightarrow 6_1^+$ transitions in ^{210}Pb (^{210}Po) with the same value of the effective neutron (proton) charge [46]. Consequently, it is also not possible to describe the decay rates along the yrast sequence in ^{212}Po with a single set of effective charges [47]. For the magnetic properties in the ^{208}Pb region the situation is not much better. It was shown that calculations using the KHPE interaction and the effective magnetic moments proposed by Arima *et al.* [42] are very successful in reproducing the static magnetic moments of many states in the region, while the calculated $M1$ transition strengths often underestimate the experimental values (see Ref. [46] and references therein). The effective charges and moments used in the present work constitute, in combination with the KHPE interaction, a standard choice in the region north-east of ^{208}Pb. However, one should keep in mind the involved uncertainties. Note that, for the new H208 interaction, a set of effective moments was determined by adjusting the calculated static moments to the available experimental information.

The results of the shell-model calculations performed with the two different effective interactions for the excited states of interest are summarized in Table II. Theoretical branching ratios were calculated using the experimental γ-ray energies. Very good agreement is found between the experimentally observed and the calculated decay pattern for the well-established $2_{2,3,4}^+$ states, which all mainly decay to the 2_1^+ level. In contrast, both calculations fail to reproduce the strong ground-state decay of the 1_1^+ state. However, the calculated transition probabilities for all decay branches of this particular level are very small. Consequently, the decay pattern is very difficult to predict. The same is true for the 3_1^+ state, for which the two calculations predict different dominant decay branches. The suggestion of $J^\pi = (3^+)$ for the 1898-keV state is therefore exclusively based on the excitation energy systematics shown in Fig. 13(a). In contrast, $J^\pi = (4^+)$ for the 2085-keV level is supported by the decay pattern predicted for the 4_4^+ state.

For the calculated $4_{2,3}^+$, $6_{2,3}^+$, and $8_{2,3}^+$ states, which are close in energy to the supposed negative-parity α-cluster states, i.e., the UPD with spins of 4^-, 6^-, and 8^- in Refs. [4,5], both SM calculations consistently predict dominant $\Delta J = 0$ decay branches to the yrast states of the same spin. This is in full accordance with the observed decay of these states. Experimental upper limits for the intensities of the nonobserved decay branches to the $J-2$ yrast states, relative to the strongest decay branch of each state, are quoted in the last column of Table II. Note that the nonobservation of these transitions also in the high-statistics experiment reported in Ref. [5] suggests that their intensities are most probably significantly smaller than the quoted limits determined from the present work. The calculated excitation energies are included in the third column of Table II. They show that the average difference between the calculated $4_{2,3}^+$, $6_{2,3}^+$, and $8_{2,3}^+$ energies and those of the UPD amounts to 61 keV (36 keV) when the KHPE (H208) effective interaction is used. It is worth noting that all conclusions drawn in this section based on the comparison between experimental information and the results of shell-model calculations do not depend on the choice of the effective interaction. The KHPE and H208 interactions discussed here, and also the interaction derived by the Naples group [48], provide results which are in full qualitative agreement.

The character of the $2_{1,2}^+$ states in ^{212}Po was already investigated in detail in Ref. [45]. In that work, the measured transition strength of $B(M1; 2_2^+ \rightarrow 2_1^+) = 0.126(16)\ \mu_N^2$ was interpreted as evidence for the isovector nature of the 2_2^+ state. The structure of the yrast and yrare 2^+ states was analyzed in a simple single-j shell-model calculation, indicating that the wave functions of these two states are dominated by only two components, namely, the $|^{210}\text{Po}, 0_1^+\rangle \otimes |^{210}\text{Pb}; 2^+\rangle$ two-neutron and the $|^{210}\text{Po}, 2^+\rangle \otimes |^{210}\text{Pb}; 0_1^+\rangle$ two-proton states, which exhaust 87% and 93%, respectively, of the total wave functions. In particular, it was shown that the 2_1^+ and 2_2^+ wave functions comprise a significant component of the fully symmetric and mixed-symmetry states, respectively.

Here, we presented shell-model calculations in a larger configuration space which consists of a whole major oscillator shell for both protons and neutrons. Extending the study presented by Kocheva *et al.* [45], we list in Table III the coefficients of the yrast and yrare wave functions in terms of the basis states $|^{210}\text{Po}, 0_1^+\rangle \otimes |^{210}\text{Pb}; J\rangle$ and $|^{210}\text{Po}, J\rangle \otimes |^{210}\text{Pb}; 0_1^+\rangle$ deduced from the calculations with the KPHE interaction. In addition, the contributions of these two components as well as those of pure fully symmetric (FSS) and mixed-symmetry states (MSS) to the total wave function are quoted. Table III shows that the enlargement of the model space does not modify the character of the 2_1^+ and 2_2^+ states. Interestingly, the properties of these states are nearly conserved for the yrast and yrare states of higher spin. In all cases, the two-neutron and two-proton basis states together amount to a large fraction of the total wave function (with $>70\%$) and appear in the yrast and yrare states as a symmetric and antisymmetric combination, respectively. Furthermore, a significant percentage of the FSS is found in the yrast states while the yrare ones are dominated by the MSS. This indicates the isovector character of the yrare states, although, because of the unbalanced superposition of the two-neutron and two-proton components, they cannot completely be identified as pure mixed-symmetry states.

The measured transition strength between the 2^+ states, $B(M1; 2_2^+ \rightarrow 2_1^+) = 0.126(16)\ \mu_N^2$, lies between the values predicted by the two SM calculations, i.e., $B(M1) = 0.35\ \mu_N^2$

TABLE II. Experimental and calculated decay properties of the excited states in ^{212}Po relevant for the present work. The results of SM calculations using either the KHPE interaction and $e_\pi = 1.5e$, $e_\nu = 0.8e$, $g_l^\pi = 1.13$, $g_s^\pi = 3.536$, $g_l^\nu = -0.08$, $g_s^\nu = -2.026$ or the H208 interaction and $e_\pi = 1.5e$, $e_\nu = 0.5e$, $g_l^\pi = 0.851$, $g_s^\pi = 5.426$, $g_l^\nu = 0.004$, $g_s^\nu = -1.024$ are shown in the columns 7–9 and 10–12, respectively. Only decay paths with branching ratios $b > 5\%$, in either the experiment or the calculations, are included. The UPD states, which in the present work are proposed to have positive parity, are printed in bold. Upper limits for the intensity of the unobserved $E2$ decay branches to the $J_i - 2$ yrast states, in percent relative to the strongest decay branch, are quoted in the last column.

						KHPE			H208			Experimental	
J_i^π	E_i^{expt} (keV)	E_i^{KH}/E_i^{H208} (keV)	J_f^π	E_f^{expt} (keV)	E_γ^{expt} (keV)	$B(E2)$ (e^2fm^4)	$B(M1)$ (μ_N^2)	b (%)	$B(E2)$ (e^2fm^4)	$B(M1)$ (μ_N^2)	b (%)	$B(M1)$ (μ_N^2)	b[a] (%)
2_2^+	1513	1430/1460	0_1^+	0	1513	91.1		23	64.3		42		21(2)
			2_1^+	727	786	0.036	0.351	77	14.1	0.0996	58	0.126(16)[b]	79(2)
1_1^+	1621	1515/1653	0_1^+	0	1621		0.0001	30		0.0008	26		79(1)
			2_1^+	727	894	1.4	0.001	68	1.9	0.0135	74		21(1)
2_3^+	1679	1714/1641	0_1^+	0	1679	24.2		44	33.6		46		26(7)
			2_1^+	727	952	25.9	0.031	56	440.2	0.014	54	0.042(20)[b]	74(7)
4_2^+	**1744**	1670/1711	2_1^+	727	1017	59.4		3	71.7		9		<13[c]
			4_1^+	1132	612	0.89	**0.735**	**97**	2.39	**0.234**	**91**	**0.52(24)**[d]	**100**
8_2^+	**1751**	1732/1798	6_1^+	1355	396	17.8			25.4				<5[c]
			8_1^+	1475	276	10.5	**1.112**	**100**	61.8	**1.3698**	**100**	**5.6(40)**[d]	**100**
6_2^+	**1787**	1718/1821	4_1^+	1132	655	32.7			64.4		2		<12[c]
			6_1^+	1355	432	3.5	**0.959**	**100**	17.7	**0.399**	**98**	**1.57(36)**[d]	**100**
2_4^+	1806	1881/1877	0_1^+	0	1806	37.3		44	0.91		8		14(3)
			2_1^+	727	1079	592.9	0.002	56	145.9		92		86(3)
3_1^+	(1898)	1858/1945	2_1^+	727	1171	1.4	0.0016	49	0.31		2		100
			4_1^+	1132	766	2.6	0.0005	5	1.1	0.0096	98		
			2_2^+	1513	385	35.2	0.006	7	29.2				
			2_3^+	1679	219	154.2	0.208	39	49.2	0.0013			
4_3^+	**1946**	2005/1984	2_1^+	727	1219	17.6		22	15.9		10		<11[c]
			4_1^+	1132	814	22.4	**0.020**	**77**	177.5	**0.043**	**90**	**0.23(11)**[d]	**100**
8_3^+	**1986**	1908/1969	6_1^+	1355	631	7.9			0.8				<21[c]
			8_1^+	1475	511	8.2	**0.142**	**99**	3.1	**0.0425**	**70**	**0.043(5)**[d]	**87(7)**
			8_2^+	1751	235	31.6	0.005		3.1	0.184	30		13(7)
6_3^+	**2016**	2082/2065	4_1^+	1132	884	26.3		5	16.7		2		<17[c]
			6_1^+	1355	661	17.0	**0.066**	**93**	69.5	**0.1187**	**98**	**0.4(2)**[d]	**100**
4_4^+	(2085)	2224/2192	2_1^+	727	1358	6.8		11	0.04				18(9)
			4_1^+	1132	953	288.6	0.002	83	147.7	0.015	100		82(9)
10_2^+	2465	2475/2555	8_1^+	1475	990	165.1		34	234.3		33		
			10_1^+	1832	633	0.24	0.077	62	0.03	0.1264	67	0.37(13)[d]	100

[a]Taken from the present work for the 1898- and 2085-keV states and from Ref. [25] for all others.
[b]Taken from Ref. [45].
[c]Upper intensity limit for unobserved transitions relative to the strongest decay branch determined from the present experiment.
[d]Calculated from the lifetimes reported in Ref. [5] assuming pure $M1$ transitions.

and $B(M1) = 0.10\ \mu_N^2$ for KHPE and H208, respectively. As can be read from Table II, significantly larger $M1$ strengths are predicted, and also experimentally determined, for the $6_2^+ \to 6_1^+$ and $8_2^+ \to 8_1^+$ transitions. Note that $M1$ strengths in the order of 1 μ_N^2 would be among the largest known all over the chart of nuclides [49].

Given the dominance of the two components mentioned above in the wave functions of all states under study, the following simple consideration can serve as a plausibility check. For each spin J, the yrast (J_1) and yrare (J_2) states can be written as

$$
\begin{aligned}
|\,^{212}\text{Po}; J_1\rangle &= |a|\,|\,^{210}\text{Pb}; J\rangle \otimes |\,^{210}\text{Po}; 0_1^+\rangle + |b|\,|\,^{210}\text{Pb}; 0_1^+\rangle \otimes |\,^{210}\text{Po}; J\rangle + \cdots, \\
|\,^{212}\text{Po}; J_2\rangle &= -|b'|\,|\,^{210}\text{Pb}; J\rangle \otimes |\,^{210}\text{Po}; 0_1^+\rangle + |a'|\,|\,^{210}\text{Pb}; 0_1\rangle \otimes |\,^{210}\text{Po}; J\rangle + \cdots,
\end{aligned} \tag{3}
$$

where $|a|, |a'| > |b|, |b'|$. The ellipsis stands for the missing minor components. Then, using tensor algebra properties, the $M1$ transition connecting the two states of Eq. (3) can be written in terms of the magnetic moments μ of the first J states in ^{210}Pb

and ^{210}Pb:

$$\langle ^{212}\mathrm{Po}; J_1||M1||\,^{212}\mathrm{Po}; J_2\rangle = \frac{\sqrt{3}}{\sqrt{4\pi}}\frac{\sqrt{J(2J+1)(J+1)}}{J}[-|ab'|\mu(^{210}\mathrm{Pb}; J) + |a'b|\,\mu\big(^{210}\mathrm{Po}; J\big)] + \cdots . \quad (4)$$

The magnetic moments of the 6^+ and 8^+ states in ^{210}Po and ^{210}Pb are experimentally known, namely, $\mu(6^+) = 5.48(5)\ \mu_N$ and $\mu(8^+) = 7.13(5)\ \mu_N$ for ^{210}Po, and $\mu(6^+) = -1.87(9)\ \mu_N$ and $\mu(8^+) = -2.45(6)\ \mu_N$ for ^{210}Pb [28]. With these experimental values one obtains

$$\begin{aligned}\langle ^{212}\mathrm{Po}; 6_1^+||M1||\,^{212}\mathrm{Po}; 6_2^+\rangle &= 1.90[1.87|ab'| + 5.48|a'b|] + \cdots ,\\ \langle ^{212}\mathrm{Po}; 8_1^+||M1||\,^{212}\mathrm{Po}; 8_2^+\rangle &= 2.14[2.49|ab'| + 7.13|a'b|] + \cdots . \end{aligned} \quad (5)$$

Based on the wave-function coefficients for the $6^+_{1,2}$ and $8^+_{1,2}$ states reported in Table III, the following estimates for the $M1$ transition strengths can be derived:

$$\begin{aligned} B(M1; 6_2^+ \rightarrow 6_1^+) &= 0.66\ \mu_N^2,\\ B(M1; 8_2^+ \rightarrow 8_1^+) &= 0.49\ \mu_N^2. \end{aligned} \quad (6)$$

The values obtained from this simple estimate are in qualitative agreement with the large strengths predicted by the shell-model calculations and those deduced from the measured lifetimes assuming pure $M1$ transitions, see Table II. In view of these results, it would certainly be of great interest to measure the lifetimes of the yrare states with higher precision, which, combined with an experimental determination of the mixing ratios, $\delta(E2/M1)$, of the dipole transitions, would allow for a more stringent test of the theoretical calculations.

To summarize this section, both the excitation energies and the decay properties of all members of the supposed UPD are in nice agreement with the results of shell-model calculations if positive parity is assumed.

D. Population of excited states via the α-transfer reaction

As discussed in Sec. V A, based on the available experimental information, none of the newly observed states in ^{212}Po can be considered as a candidate for the collective $J^\pi = 2^-$ states predicted by α-cluster theory [6,7]. The main argument put forward here is that the new levels are populated with much smaller exclusive cross sections as compared with the supposed negative-parity doublet states. In Fig. 14, we show the exclusive cross sections for the population of excited states in ^{212}Po via α-transfer determined in the present work. In Fig. 14(a), they are shown for positive-parity yrare states including the newly identified (3_1^+) level. Figure 14(b) presents the cross sections for the negative-parity yrast band (blue in Figs. 10 and 13). The cross sections determined for the UPD, whose parity is under debate, are included in both parts of the figure. At negative parity, the values for the members of the $\nu 1g_{9/2} \times 0j_{15/2}$ multiplet exhibit a strong odd-even staggering. This reflects the well-known preference for the population of natural-parity states, i.e., odd spins for negative parity, in transfer reactions. Assuming that the supposed UPDs actually correspond to the calculated $4^+_{2,3}$, $6^+_{2,3}$, and $8^+_{2,3}$ shell-model states (see Fig. 13), the exclusive cross sections measured for the states belonging to the $\nu 1g_{9/2} \times 0i_{11/2}$ multiplet show a strong staggering, indicating again the preference for the population of natural-parity states, in this case those of even spin. Unfortunately, the determination of reliable cross sections for the 8^+_2 and 10^+_1 states is difficult because these states directly populate the 8^+_1 isomer. As a consequence, their intensities have to be determined from the singles γ-ray spectrum in

TABLE III. Wave-function decomposition for the yrast and yrare $J^\pi = 2^+$, 4^+, 6^+, and 8^+ states in ^{212}Po. The coefficients of the wave functions in terms of the basis states $|\,^{210}\mathrm{Po}, 0_1^+\rangle \otimes |\,^{210}\mathrm{Pb}; J\rangle$ (labeled two-neutron) and $|\,^{210}\mathrm{Po}, J\rangle \otimes |\,^{210}\mathrm{Pb}; 0_1^+\rangle$ (labeled two-proton) are quoted in the second and third columns, respectively. The summed contribution of these two components, as well as those of the full symmetric (FSS) and mixed-symmetry states (MSS), to the total wave function are given in last three columns.

J_i^π	Two-neutron	Two-proton	Fraction (%)	FSS (%)	MSS (%)
2_1^+	0.80	0.42	82	74	7
4_1^+	0.83	0.30	78	64	14
6_1^+	0.88	0.22	83	61	22
8_1^+	0.90	0.14	83	54	29
2_2^+	−0.43	0.75	75	5	70
4_2^+	−0.39	0.81	81	9	72
6_2^+	−0.30	0.87	85	16	68
8_2^+	−0.24	0.81	71	16	55

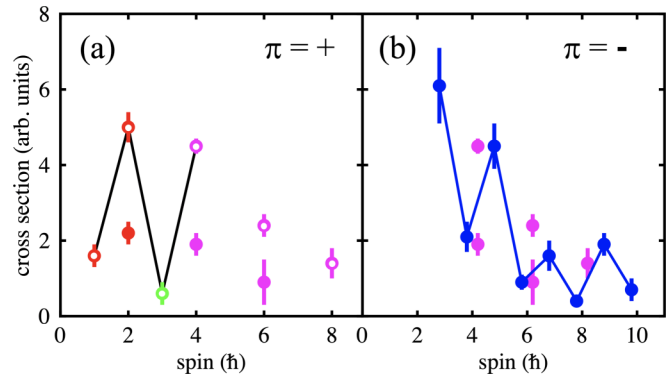

FIG. 14. Exclusive reaction cross sections in arbitrary units for the strongly populated (a) positive-parity yrare and (b) negative-parity yrast states in ^{212}Po. The values for the UPD are included in both panels. The color code is the same as the one employed in Figs. 10 and 13 and known states with firm spin assignment are shown in red. Members of the $\nu 1g_{9/2} \times 0i_{11/2}$ multiplet are marked by white dots and connected by black lines.

which the relevant lines are unfortunately all contaminated by transitions belonging to ^{211}Po. Interestingly, Fig. 14(a) shows that, despite their higher excitation energies, the members of the neutron $1g_{9/2} \times 0i_{11/2}$ multiplet receive a stronger population as compared with the states of the same spin belonging to the proton $0h_{9/2}^2$ configuration. Although the cross-section systematics shown in Fig. 14 cannot be considered as a proof for positive parity of the supposed UPD, it shows that this assumption leads to a consistent picture with respect to the population of excited states in the α-transfer reaction employed in the present work.

VI. CONCLUSIONS

We reported on the results of a γ-ray spectroscopic study of ^{212}Po in which excited states were populated in an α-transfer reaction and the γ rays emitted in their decay detected by the AGATA array. An analysis of particle-γ and -$\gamma\gamma$ coincidences enabled the identification of 14 new excited states in the energy range between 1.9 and 3.3 MeV and a tentative spin assignment for two of them. Despite the selectivity provided by the reaction mechanism and the experimental setup, no candidate for any of the $J^\pi = 2^-$ states predicted by theory at excitation energies below 2.1 MeV could be identified. An analysis of the γ-ray linear polarization, taking advantage of the position resolution of the AGATA detectors, provided clear experimental evidence for the magnetic character of one of the nonstretched dipole transitions connecting the doublet states to the ground-state band, namely, the 432-keV γ ray populating the 6_1^+ yrast state. This experimental information allowed us to firmly assign a spin-parity of 6^+ to the state at an excitation energy of 1787 keV. As discussed in the present work, the energies and decay properties of all six doublet states with spins of 4, 6, and 8, respectively, and excitation energies in the range between 1.7 and 2.1 MeV agree very well with shell-model predictions when positive parity is assumed. Such an assignment is also consistent with the measured exclusive reaction cross sections. Although this indirect information is certainly not sufficient to firmly assign positive parity to all six states, it at least seriously questions the assignment of negative parity proposed in previous work. Only a dedicated experiment to unequivocally determine the parity of all states under discussion will allow us to draw definite conclusions with respect to the interplay between α-cluster and shell-model structures in ^{212}Po.

ACKNOWLEDGMENTS

We thank the GANIL staff for the excellent technical support during the experiment and the AGATA collaboration for the very good performance of the array. This project has received funding from the European Union's Horizon 2020 research and innovation programme under Grant Agreement No. 654002 and FEDER funds. We furthermore acknowledge support from the Spanish Ministerio de Ciencia, Inovación y Universidades under contracts FPA2014-57196-C5, FPA2017-84756-C4, and SEV-2014-0398, the Generalitat Valenciana under Grant No. PROMETEO/2019/005, the Swedish Research Council (Vetenskapsrådet, VR 2016-3969), and the German BMBF under Contracts No. 05P18PKFN9 and No. 05P19PKFNA.

[1] A. R. Poletti, G. D. Dracoulis, A. P. Byrne, and A. E. Stuchbery, Nucl. Phys. A **473**, 595 (1987).
[2] K. Varga, R. G. Lovas, and R. J. Liotta, Phys. Rev. Lett. **69**, 37 (1992).
[3] B. Buck, A. C. Merchant, and S. M. Perez, Phys. Rev. Lett. **72**, 1326 (1994).
[4] A. Astier, P. Petkov, M.-G. Porquet, D. S. Delion, and P. Schuck, Phys. Rev. Lett. **104**, 042701 (2010).
[5] A. Astier, P. Petkov, M.-G. Porquet, D. S. Delion, and P. Schuck, Eur. Phys. J. A **46**, 165 (2010).
[6] Y. Suzuki and S. Ohkubo, Phys. Rev. C **82**, 041303(R) (2010).
[7] D. S. Delion, R. J. Liotta, P. Schuck, A. Astier, and M.-G. Porquet, Phys. Rev. C **85**, 064306 (2012).
[8] C. Rodríguez-Tajes, F. Farget, X. Derkx, M. Caamaño, O. Delaune, K.-H. Schmidt, E. Clément, A. Dijon, A. Heinz, T. Roger, L. Audouin, J. Benlliure, E. Casarejos, D. Cortina, D. Dore, B. Fernandez-Dominguez, B. Jacquot, B. Jurado, A. Navin, C. Paradela *et al.*, Phys. Rev. C **89**, 024614 (2014).
[9] C. Stahl, J. Leske, C. Bauer, D. Bazzacco, E. Farnea, A. Gottardo, P. R. John, C. Michelagnoli, N. Pietralla, M. Reese *et al.*, Phys. Rev. C **92**, 044324 (2015).
[10] R. Bass, *Nuclear Reactions with Heavy Ions* (Springer, New York, 1980).
[11] D. C. Biswas, R. K. Choudhury, B. K. Nayak, D. M. Nadkarni, and V. S. Ramamurthy, Phys. Rev. C **56**, 1926 (1997).
[12] F. Videbaek, R. B. Goldstein, L. Grodzins, S. G. Steadman, T. A. Belote, and J. D. Garrett, Phys. Rev. C **15**, 954 (1977).
[13] W. R. Phillips, Rep. Prog. Phys. **40**, 345 (1977).
[14] D. C. Rafferty, M. Dasgupta, D. J. Hinde, C. Simenel, E. C. Simpson, E. Williams, I. P. Carter, K. J. Cook, D. H. Luong, S. D. McNeil, K. Ramachandran, K. Vo-Phuoc, and A. Wakhle, Phys. Rev. C **94**, 024607 (2016).
[15] M. Wang, G. Audi, F. G. Kondev, W. J. Huang, S. Naimi, and X. Xing, Chin. Phys. C **41**, 030003 (2017).
[16] P. Banerjee, S. Ganguly, M. K. Pradhan, Md. Moin Shaikh, H. P. Sharma, S. Chakraborty, R. Palit, R. G. Pillay, V. Nanal, S. Saha, J. Sethi, and D. C. Biswas, Phys. Rev. C **92**, 024318 (2015).
[17] S. Akkoyun *et al.*, Nucl. Instrum. Methods Phys. Res., Sect. A **668**, 26 (2012).
[18] E. Clément, C. Michelagnoli, G. de France, H. J. Li, A. Lemasson, C. Barthe Dejean, M. Beuzard, P. Bougault, J. Cacitti, J.-L. Foucher *et al.*, Nucl. Instrum. Methods Phys. Res., Sect. A **855**, 1 (2017).
[19] J. Ljungvall, R. M. Pérez-Vidal, A. Lopez-Martens, C. Michelagnoli, E. Clément, J. Doudouet, A. Gadea, H. Hess, A. Korichi, M. Labiche *et al.*, Nucl. Instrum. Methods Phys. Res., Sect. A **955**, 163297 (2020).

[20] P. Golubev, P. Kristiansson, N. Arteaga-Marrero, M. Elfman, K. Malmqvist, E. J. C. Nilsson, C. Nilsson, J. Pallon, and M. Wegdén, Nucl. Instrum. Methods Phys. Res., Sect. B **267**, 2065 (2009).
[21] B. Bruyneel, P. Reiter, A. Wiens, J. Eberth, H. Hess, G. Pascovici, N. Warr, S. Aydin, D. Bazzacco, and F. Recchia, Nucl. Instrum. Methods Phys. Res., Sect. A **608**, 99 (2009).
[22] B. Bruyneel, B. Birkenbach, J. Eberth, H. Hess, Gh. Pascovivi, P. Reiter, A. Wiens, D. Bazzacco, E. Farnea, C. Michelagnoli, and F. Recchia, Eur. Phys. J. A **49**, 61 (2013).
[23] A. Lopez-Martens, K. Hauschild, A. Korichi, J. Roccaz, and J.-P. Thibaud, Nucl. Instrum. Methods Phys. Res., Sect. A **533**, 454 (2004).
[24] A. Fernández Martínez, Ph.D. thesis, Universidad Autónoma de Madrid, 2021 (unpublished).
[25] K. Auranen and E. A. McCutchan, Nucl. Data Sheets **168**, 117 (2020).
[26] P. J. Siemens, J. P. Bondorf, D. H. E. Gross, and F. Dickmann, Phys. Lett. B **36**, 24 (1971).
[27] D. Chattopadhyay, S. Santra, A. Pal, A. Kundu, K. Ramachandran, R. Tripathi, D. Sarkar, S. Sodaye, B. K. Nayak, A. Saxena, and S. Kailas, Phys. Rev. C **94**, 061602(R) (2016).
[28] http://www.nndc.bnl.gov/ensdf.
[29] J. R. Cottle, Vandana Tripathi, B. A. Brown, B. Abromeit, J. M. Allmond, M. Anastasiou, L. T. Baby, J. S. Baron, P. D. Cottle, R. Dungan, T. C. Hensley, K. W. Kemper, R. S. Lubna, N. Rijal, E. Rubino, S. L. Tabor, P. L. Tai, K. Villafana, and I. Wiedenhoever, Phys. Rev. C **95**, 064323 (2017).
[30] B. Alikhani, A. Givechev, A. Heinz, P. R. John, J. Leske, M. Lettmann, O. Möller, N. Pietralla, and C. Röder, Nucl. Instrum. Methods Phys. Res., Sect. A **675**, 144 (2012).
[31] T. Aoki, K. Furuno, Y. Tagishi, S. Ohya, and J.-Z. Ruan, At. Data Nucl. Data Tables **23**, 349 (1979).
[32] D. M. Brink, Phys. Lett. B **40**, 37 (1972).
[33] N. Anyas-Weiss, J. C. Cornell, P. S. Fisher, P. N. Hudson, A. Menchaca-Rocha, D. J. Millener, A. D. Panagiotou, D. K. Scott, D. Strottman, D. M. Brink *et al.*, Phys. Rep. **12**, 201 (1974).
[34] P. von Neumann-Cosel, P. Schenk, U. Fister, T. K. Trelle, and R. Jahn, Phys. Rev. C **47**, 1027 (1993).
[35] M. Piiparinen, P. Kleinheinz, S. Lunardi, M. Ogawa, G. de Angelis, F. Soramel, W. Meczynski, and J. Blomqvist, Z. Phys. A **337**, 387 (1990).
[36] E. Caurier, shell-model code ANTOINE (IRES, Strasbourg, 1989–2002).
[37] E. Caurier and F. Nowacki, Acta Phys. Pol. **30**, 705 (1999).
[38] G. H. Herling and T. T. S. Kuo, Nucl. Phys. A **181**, 113 (1972).
[39] E. K. Warburton and B. A. Brown, Phys. Rev. C **43**, 602 (1991).
[40] H. Naïdja, Phys. Scr. **94**, 014005 (2019).
[41] H. Naïdja, Phys. Rev. C **103**, 054303 (2021).
[42] A. Arima, K. Shimizu, W. Bentz, and H. Hyuga, in *Advances in Nuclear Physics*, edited by E. Vogt and J. W. Negele (Plenum, New York, 1987), Vol. 18.
[43] R. Broda, L. W. Iskra, R. V. F. Janssens, B. A. Brown, B. Fornal, J. Wrzesinski, N. Cieplicka-Orynczak, M. P. Carpenter, C. J. Chiara, C. R. Hoffman, F. G. Kondev, G. J. Lane, T. Lauritsen, Z. Podolyak, D. Seweryniak, W. B. Walters, and S. Zhu, Phys. Rev. C **98**, 024324 (2018).
[44] E. Dupont, A. Astier, C. M. Petrache, B. F. Lv, I. Deloncle, J. Kiener, R. Orlandi, H. Makii, K. Nishio, K. Hirose, M. Asai, T. K. Sato, K. Tsukada, Y. Ito, K. R. Kean, R. Yanagihara, and G. Scamps, Phys. Rev. C **101**, 014309 (2020).
[45] D. Kocheva, G. Rainovski, J. Jolie, N. Pietralla, C. Stahl, P. Petkov, A. Blazhev, A. Hennig, A. Astier, Th. Braunroth, M. L. Cortes, A. Dewald, M. Djongolov, C. Fransen, K. Gladnishki, V. Karayonchev, J. Litzinger, C. Muller-Gatermann, M. Scheck, P. Scholz *et al.*, Phys. Rev. C **93**, 011303(R) (2016).
[46] V. Karayonchev, A. Blazhev, A. Esmaylzadeh, J. Jolie, M. Dannhoff, F. Diel, F. Dunkel, C. Fransen, L. M. Gerhard, R.-B. Gerst, L. Knafla, L. Kornwebel, C. Muller-Gatermann, J. M. Regis, N. Warr, K. O. Zell, M. Stoyanova, and P. VanIsacker, Phys. Rev. C **99**, 024326 (2019).
[47] D. Kocheva, G. Rainovski, J. Jolie, N. Pietralla, A. Blazhev, R. Altenkirch, S. Ansari, A. Astier, M. Bast, M. Beckers, T. Braunroth, M. Cappellazzo, A. Dewald, F. Diel, M. Djongolov, C. Fransen, K. Gladnishki, A. Goldkuhle, A. Hennig, V. Karayonchev *et al.*, Phys. Rev. C **96**, 044305 (2017).
[48] L. Coraggio, A. Covello, A. Gargano, and N. Itaco, Phys. Rev. C **80**, 021305(R) (2009).
[49] P. M. Endt, At. Data Nucl. Data Tables **26**, 47 (1981).